J. Fluid Mech. (1998), *vol.* 377, *pp.* 267–312. Printed in the United Kingdom

Laminar–turbulent transition in pipe flow for Newtonian and non-Newtonian fluids

By A. A. DRAAD†, G. D. C. KUIKEN AND F. T. M. NIEUWSTADT‡

J.M. Burgers Centre, Delft University of Technology,
Rotterdamseweg 145, 2628 AL Delft, the Netherlands

(Received 10 February 1998 and in revised form 27 July 1998)

A cylindrical pipe facility with a length of 32 m and a diameter of 40 mm has been designed. The natural transition Reynolds number, i.e. the Reynolds number at which transition occurs as a result of non-forced, natural disturbances, is approximately 60 000. In this facility we have studied the stability of cylindrical pipe flow to imposed disturbances. The disturbance consists of periodic suction and injection of fluid from a slit over the whole circumference in the pipe wall. The injection and suction are equal in magnitude and each distributed over half the circumference so that the disturbance is divergence free. The amplitude and frequency can be varied over a wide range.

First, we consider a Newtonian fluid, water in our case. From the observations we compute the critical disturbance velocity, which is the smallest disturbance at a given Reynolds number for which transition occurs. For large wavenumbers, i.e. large frequencies, the dimensionless critical disturbance velocity scales according to Re^{-1}, while for small wavenumbers, i.e. small frequencies, it scales as $Re^{-2/3}$. The latter is in agreement with weak nonlinear stability theory. For Reynolds numbers above 30 000 multiple transition points are found which means that increasing the disturbance velocity at constant dimensionless wavenumber leads to the following course of events. First, the flow changes from laminar to turbulent at the critical disturbance velocity; subsequently at a higher value of the disturbance it returns back to laminar and at still larger disturbance velocities the flow again becomes turbulent.

Secondly, we have carried out stability measurements for (non-Newtonian) dilute polymer solutions. The results show that the polymers reduce in general the natural transition Reynolds number. The cause of this reduction remains unclear, but a possible explanation may be related to a destabilizing effect of the elasticity on the developing boundary layers in the entry region of the flow. At the same time the polymers have a stabilizing effect with respect to the forced disturbances, namely the critical disturbance velocity for the polymer solutions is larger than for water. The stabilization is stronger for fresh polymer solutions and it is also larger when the polymers adopt a more extended conformation. A *delay* in transition has been only found for extended fresh polymers where *delay* means an increase of the critical Reynolds number, i.e. the number below which the flow remains laminar at any imposed disturbance.

---

† Current address: Océ Research, Venlo, the Netherlands.
‡ Author to whom correspondence should be addressed: e-mail f.nieuwstadt@wbmt.tudelft.nl.

1. Introduction

Research on transition to turbulence in a cylindrical pipe goes back more than one-hundred years to 1883 when Osborne Reynolds performed his famous experiments. He found that a laminar flow of a Newtonian fluid in a pipe becomes unstable if the dimensionless number which nowadays carries his name exceeds a certain critical value. Even today, his finding has not been explained satisfactorily by theory and we still know relatively little about the processes and mechanisms involved in the transition of cylindrical pipe flow. This classical problem is to be considered as still open.

In contrast, for the related flow geometry of plane Poiseuille flow, stability theory is fairly well developed. The existence of linear instabilities known as Tollmien–Schlichting waves has been established and these have been also confirmed experimentally by Nishioka, Iida & Ichikawa (1975). When these linear instabilities grow large enough, nonlinear effects become important. Secondary instabilities emerge in the form of lambda-vortex patterns and they are known as Klebanov-modes and Herbert-modes (Herbert 1983). These lambda-vortex patterns have been visualized in experiments (Kozlov & Ramazanov 1984*a*, *b*) and have also been found in numerical simulations (Kleiser & Zhang 1991).

The scenario of linear and secondary instabilities found for plane Poiseuille flow is inappropriate for cylindrical pipe flow since this flow is believed to be stable for all infinitesimal perturbations (Drazin & Reid 1981). In recent years, other instability mechanisms have been put forward which can provide a possible explanation for transition in pipe flow. One of these is transient growth (Trefethen *et al.* 1993). By transient growth, disturbances that are in principle linearly stable can nevertheless grow initially in magnitude before finally decaying (O'Sullivan & Breuer 1994*a*). Bergström (1993) has shown analytically that for pipe flow the largest amplification through transient growth is obtained for disturbances with streamwise wavenumber α equal to zero and with an azimuthal wavenumber equal to unity. Axisymmetric disturbances, i.e. azimuthal wavenumber equal to zero, display almost no transient growth. The transient growth which can be as large as four to five orders of magnitude, attains a maximum at dimensionless times $t/Re \approx 0.05$. The amplitude magnification scales with Reynolds number, Re, both for $\alpha = 0$ and for non-zero α. Schmid & Henningson (1994) construct the linear disturbance that gives the maximum possible transient growth but its shape is rather complex and difficult to realize in an experiment. To continue into the nonlinear range, O'Sullivan & Breuer (1994*b*) perform a direct numerical simulation of a pipe flow at $Re = 2200$. They can generate transition and find a structure resembling a puff. However, the Reynolds number is too low and the flow seems to decay to a laminar state.

Tumin (1996) has investigated the linear receptivity problem for cylindrical pipe flow by considering the response to a disturbance which consists of periodic injection and suction from a narrow slit in the pipe wall. Various azimuthal distributions of injection/suction have been considered. It is found that the disturbance primarily excites modes with a large contribution near the pipe wall whereas the least stable linear modes have their main contribution in the pipe centre. In a subsequent paper by Eliahou, Tumin & Wygnanski (1998) it is suggested that a so-called self-sustained process (SSP) introduced by Waleffe (1997), may be the appropriate process to explain transition in pipe flow. In this process a key role is played by self-sustained axial vortices which have been observed in numerical simulations of transitional pipe flow (Hua, Zhang & Nieuwstadt 1998).

Besides this theoretical progress, there have been also advances made based on experimental work. The most extensive experiments have been carried out by Wygnanski and coworkers (Wygnanski & Champagne 1973; Wygnanski, Solokov & Friedman 1975 and Rubin, Wygnanski & Haritonidis 1980). They identify two types of structures in transitional pipe flow which they call puffs and slugs. The difference between these two structures is given by the behaviour of the velocity near the leading edge, with a puff displaying a more gradual change of velocity near the leading edge and with a more discontinuous change for a slug. Puffs are found for $Re < 2800$ and they decay below $Re \approx 2200$. Turbulent slugs appear for $Re \geqslant 3000$. The growth of puffs above $Re \approx 2300$ seems to be in agreement with the simulation results of O'Sullivan & Breuer (1994*b*) mentioned above. Additional results on the puff and slug structure have been obtained by Hua *et al.* (1998) by means of numerical simulations. The experiments of Wygnanski *et al.* cited above have been carried out for a constant-pressure-gradient flow. Recently, Darbyshire & Mullin (1995) extended this work to a constant-mass-flux flow. The same two types of structures are observed. Moreover, it is found in this latter case that below $Re \approx 1760$ no turbulent structures can be sustained.

The change from laminar to turbulent flow is accompanied by a large change in flow-related processes such as mixing, heat transfer and drag which all increase dramatically. This has for instance important consequences for various industrial applications in which transitional pipe flow is encountered and a correct prediction of the transition in this case is very important. Keeping industrial applications in mind, we are faced with another problem. Until now we have limited our discussion, without explicitly saying so, to Newtonian fluids, i.e. all experimental and theoretical results quoted above have been obtained for these fluids. In industrial applications, however, one frequently uses fluids which can be characterized as non-Newtonian. Therefore, it seems appropriate to consider also the effect of non-Newtonian behaviour on the transition process.

A particular type of non-Newtonian fluid is formed by a Newtonian solvent in which one dissolves a small amount of polymer with a high molecular weight. In turbulent flow, the conformation, i.e. the shape of the polymer, appears to have a large influence on the turbulence structure. One of the most well-known consequences is a substantial drag reduction. Virk (1975) has introduced the terms 'type-A' and 'type-B' to distinguish between the drag-reducing behaviour of randomly-coiled and linearly extended polymers, respectively. For drag-reducing polymers of type-A the transition point is located at the same Reynolds number as for the (Newtonian) solvent ($Re_c \approx 2300$). The Newtonian behaviour is followed up to the point where drag reduction starts and which is called the onset point. From this point on, the lines with different polymer concentrations fan out in a so-called Moody diagram in which the friction coefficient is plotted versus Reynolds number, with the largest drag reduction for the highest polymer concentration. In Type-B drag reduction, however, no onset point is found and drag reduction appears immediately the flow becomes turbulent. Examples of this case are fibre solutions, soaps, clays and extended polyelectrolytes. To study this different drag-reducing behaviour as a function of polymer conformation, Virk & Wagger (1990) carried out an experiment with a partially hydrolysed polyacrylamide (PAMH) of high molecular weight. In a solvent which does not contain any dissolved salt, these polymers adopt an extended conformation. Adding salt to the solution forces the polymers to assume a randomly-coiled conformation. Virk & Wagger (1990) find type-B behaviour for the experiments without salt and type-A behaviour when salt is added.

For many of these dilute polymer solutions, transition of pipe flow appears to occur at roughly the same Reynolds number as observed for Newtonian fluids (Virk *et al.* 1967). However, in some cases a delay of transition is observed, i.e. the minimum Reynolds number at which transition occurs becomes larger. When we for example correct the data of Virk & Wagger (1990) for the increase in viscosity due to the dissolved polymers, their results for the type-B case show a delay in transition to a Reynolds number of approximately 6500 (a fact which they do not mention themselves). A delay in transition has also been found for Xanthan gum (Bewersdorff & Singh 1988 and Rochefort & Middleman 1985), which has a rigid helical structure. Other examples are asbestos fibres (Vaseleski & Mezner 1974) and surfactants that form so-called rod-like micelles (Bewersdorff 1990). Some theoretical support for the result that extended polymers may cause delay transition is found in the stability analysis of a dilute suspension of slender fibres in plane Poiseuille flow which shows that the fibres have a stabilizing influence (Landahl 1973 and Bark & Tinoco 1978).

Although type-A drag-reducing polymers commonly do not show any delay in transition, a delay has nevertheless been found for high molecular weight polymers in pipes with a small diameter, typically less than 1 cm (Castro & Squire 1967; White & McEligot 1970; Chung & Graebel 1972; Wójs 1993) and for concentrated solutions of low molecular weight polymers (e.g. Sá Pereira & Pinho 1994). To complicate matters even further, transition Reynolds numbers have been found that are *smaller* than the Newtonian minimum of approximately 2300 and for this phenomenon the term 'early turbulence' has been coined. For instance, transition Reynolds numbers as low as 500 have been reported (Forame, Hansen & Little 1972; Zakin, Ni & Hansen 1977; Li & McCarthy 1995). Another result is given by Paterson & Abernathy (1972) who found that for a pipe inlet with squared corners polymers do not change the transition Reynolds number. For a smooth-nozzle inlet, however, adding polymers results in a decrease of natural transition Reynolds number below its Newtonian value of $Re \approx 10\,000$, an effect which increases with the polymer concentration.

For a theoretical approach to transition of non-Newtonian fluid flow in a cylindrical pipe, we may refer to Hansen (1973) who has performed a stability analysis of axisymmetric disturbances. The axisymmetric disturbances that he studied decay, but when the elasticity number is increased above a certain value, the decay rate becomes smaller than for disturbances in a Newtonian fluid. In other words, the effect of elasticity is destabilizing. Most other theoretical developments, however, have been done for plane Poiseuille flow. It is confirmed in this case that elasticity has a destabilizing effect, namely the critical Reynolds number above which linear disturbances can grow decreases with increasing elasticity (e.g. Walters 1962; Porteous & Denn 1972*a*; Sureshkumar & Beris 1995*b*). Whereas Porteous & Denn find a monotonic decrease of critical Reynolds number, Sureshkumar & Beris find a minimum of $Re_c \approx 1670$ where the elasticity number is $E \approx 2.5 \times 10^{-3}$. The corresponding Weissenberg number of this minimum value is $We \approx 4$, i.e. a stabilizing effect occurs for linear disturbances once the flow time scale is more than four times the relaxation time of the fluid. Porteous & Denn (1972*b*) extended their work to weakly nonlinear disturbances and also found that elasticity has a destabilizing effect on plane Poiseuille flow when compared to Newtonian fluids. Three-dimensional direct numerical simulations for visco-elastic fluids seem to become numerically unstable at high Weissenberg numbers (Sureshkumar & Beris 1995*a*; Maulik 1989).

In view of the discussion given above, the conclusion is justified that it is unclear under which circumstances transition of non-Newtonian pipe flow is different to transition for a Newtonian fluid. Therefore, the objective of our study is to throw

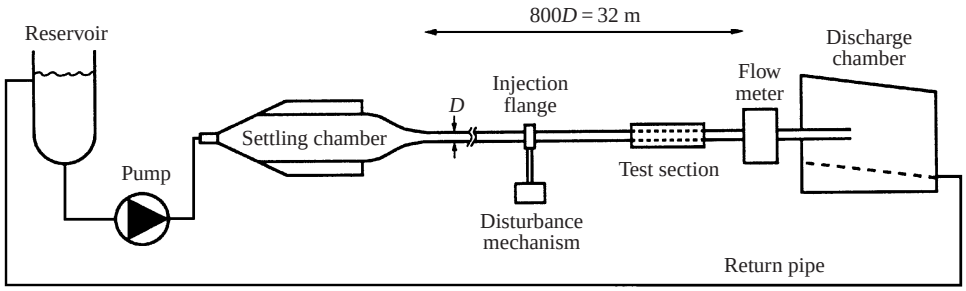

FIGURE 1. Schematic overview of the pipe-flow facility; the inner diameter of the pipe is 40 mm. Further details of this experimental facility are explained in the text.

more light on this problem. For this we carry out experiments of transitional pipe flow. It has also become clear that transition of a Newtonian fluid in a cylindrical pipe flow geometry is far from being completely documented. Therefore, we first consider experiments for the Newtonian case. Apart from providing more information on this classical transition problem, these results are also used as reference for the investigation of the effect of non-Newtonian behaviour on transition. In particular we will test the hypothesis that extended polymers are important for a delay in transition by performing stability measurements with PAMH polymers the conformation of which can be changed by varying the salt concentration.

We have organized this paper as follows. In § 2 we describe the pipe-flow facility that we designed to perform the stability measurements in water and polymer solutions. The results of the stability measurements in water are presented in § 3. The stability measurements for the polymer solutions are discussed in § 4 together with the handling of the polymers and the correction of the results for the shear-rate-dependent viscosity. In § 5 we summarize the main conclusions of our study.

2. Experimental facility

The pipe-flow facility used for our experiments has been designed especially for the purpose of studying transitional flow. This objective requires an experimental set-up in which laminar flow, preferably fully developed, can be maintained over a large range of Reynolds numbers so that the transition process can be studied as a function of varying flow conditions. In this section we give a brief description of the flow facility and for further details we refer to Draad (1996).

2.1. *Pipe-flow facility*

A schematic overview of the facility is given in figure 1. As we aim also to perform experiments with non-Newtonian fluids and since most polymers degrade when in contact with metals in general and with zinc and aluminium in particular, all parts of the facility are made out of plastic. Further details of the set-up with respect to the measurements with non-Newtonian fluids will be discussed in § 4.1.

The main part of the facility consists of a smooth-walled pipe constructed out of Plexiglas with an inner diameter of 40 mm, and a total length of 32 m. According to Christiansen & Lemmon (1965) the length after which the centreline velocity deviates by less than 1% from the parabolic form, is given by

$$\frac{L_{99\%}}{D} = 0.056\,Re. \tag{2.1}$$

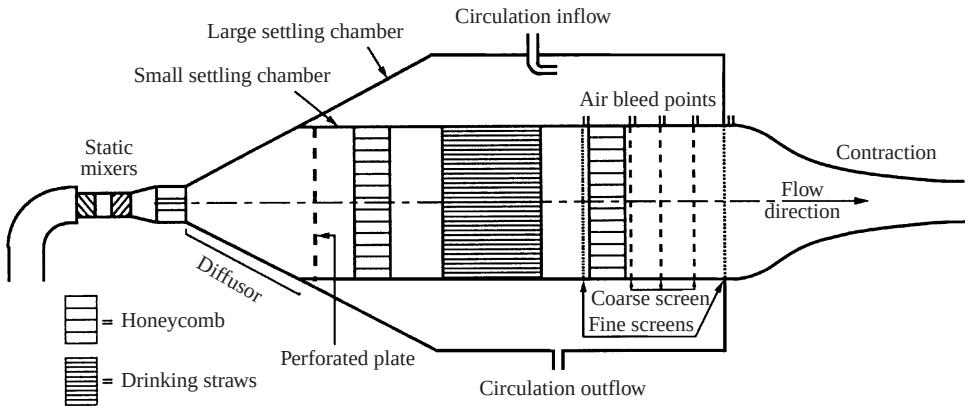

FIGURE 2. Detailed view of the settling chamber giving the position of the various screens and honeycombs in the small settling chambers. The air bleed holes are connected to the outside of the large settling chamber. This allows removal of air bubbles during circulation. The space between the small and the large settling chamber is filled with water that has the temperature of the water in the reservoir.

Based on this expression we estimate that our facility is able to sustain a fully developed, parabolic pipe flow for Reynolds numbers up to 14 300. As we shall see later, laminar flow can be maintained up to $Re = 60\,000$. Such a high value could be obtained by avoiding and/or minimizing all sources of flow disturbances during the design and construction of the pipe. The pipe is made out of 2 m long sections connected to each other by specially designed couplings. The pipe sections are centred based on their inner diameter and the ends are made slightly conical (top angle between 2° and 3°) to make the connections flush and the pipe sections interchangeable. The design of the couplings limited any misalignment of sections to less than 0.02 mm.

To eliminate flow disturbance from entering the pipe, a settling chamber has been designed. Swirl is suppressed here with the help of honeycombs and other flow disturbances are damped with a series of screens as shown in figure 2. The distance between the last coarse screen (mesh size 2 mm) and the stainless steel fine screen (mesh size 0.5 mm) is 40 mm, i.e. 20 times the mesh size. According to Groth & Johansson (1988) this is the minimum separation distance between two consecutive screens and it coincides with the region of rapid decay of turbulence intensity. A smooth contraction of area ratio 9 is used to damp the disturbances further. The shape of the contraction has been optimized to keep the adverse pressure gradient small and to minimize the Görtler number. For this we have used a design procedure based on an extension of the method proposed by Cohen & Ritchie (1962), which is based on potential-flow theory. The contour of the contraction that we use is shown in figure 3. Finally, by careful insulation of the pipe and settling chamber and also by thermostatically matching the water temperature to that of the ambient air within 0.2 °C, any disturbing influence of convection currents has been avoided.

The pipe ends in a discharge chamber from which the water returns into a reservoir to be recirculated back in the pipe.

Along the pipe, the velocity profile can be observed at any location by means of laser Doppler velocimetry (LDV). This is done by replacing a pipe section with a specially designed measuring box. This is a rectangular box which is positioned around the pipe. It is filled with water at about the same pressure as the fluid in

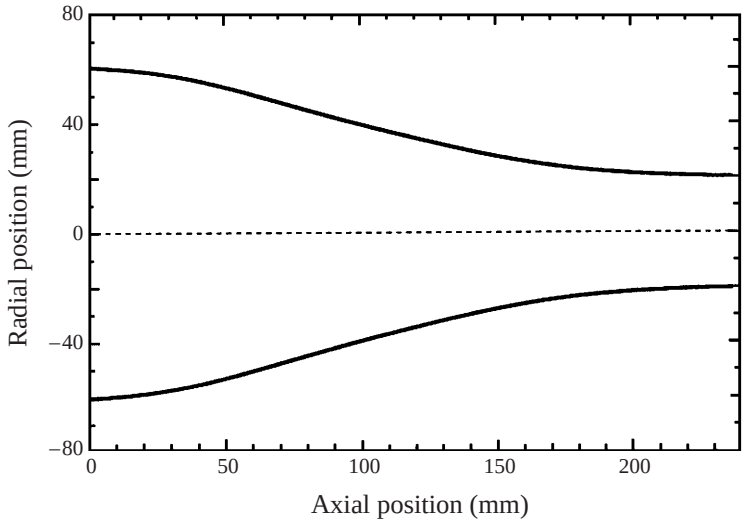

FIGURE 3. The optimized contraction contour that we use to connect the settling chamber to the pipe.

the pipe. In this box the pipe wall is replaced by a 0.19 mm thin fluorocarbon film (Teflon FEP 750A by Du Pont) with an index of refraction of 1.35, which is close to that of water (1.33). In this way refraction effects due to the curved pipe wall which lead e.g. to non-coincidence of the LDV measuring volumes, can be eliminated.

At the downstream end of the pipe (see figure 1), a magnetic inductive flow meter (Krohne-Altometer, type M950/6) is used to monitor the flow rate. The flow-meter signal is used to control the pump in order to maintain a constant flow rate even under transitional flow conditions. The flow control system is able to keep the flow rate constant within a variation of 0.5 %, also when transition to turbulence is triggered. However, when natural transition occurs, which always starts near the entrance of the pipe, the flow rate can decrease by as much as 10% at high Reynolds numbers because the increase in drag is not compensated quickly enough by increasing the rotational speed of the pump.

2.2. *Flow quality*

In this section we present some general results on the flow characteristics of our pipe facility. For this we consider the so-called Moody diagram in which the dimensionless pressure pressure gradient, i.e. the Moody† friction factor f_M, is plotted as a function of the dimensionless flow rate expressed in the form of the Reynolds number Re. Here, Re and f_M are defined as

$$Re = \frac{\rho \overline{W} D}{\eta} = \frac{\overline{W} D}{\nu}, \qquad f_M = \frac{D}{L} \frac{\Delta p}{\frac{1}{2}\rho \overline{W}^2}, \tag{2.2}$$

where ρ is the density, $\overline{W}$ is the velocity averaged over the pipe cross-section, D the pipe diameter and Δp a pressure drop over a length L along the pipe. The η and ν are the dynamic and the kinematic viscosity of the fluid respectively.

† Another commonly used definition of the friction factor is the so-called Fanning friction factor f_F, which is related to f_M: $f_M = 4 f_F$.

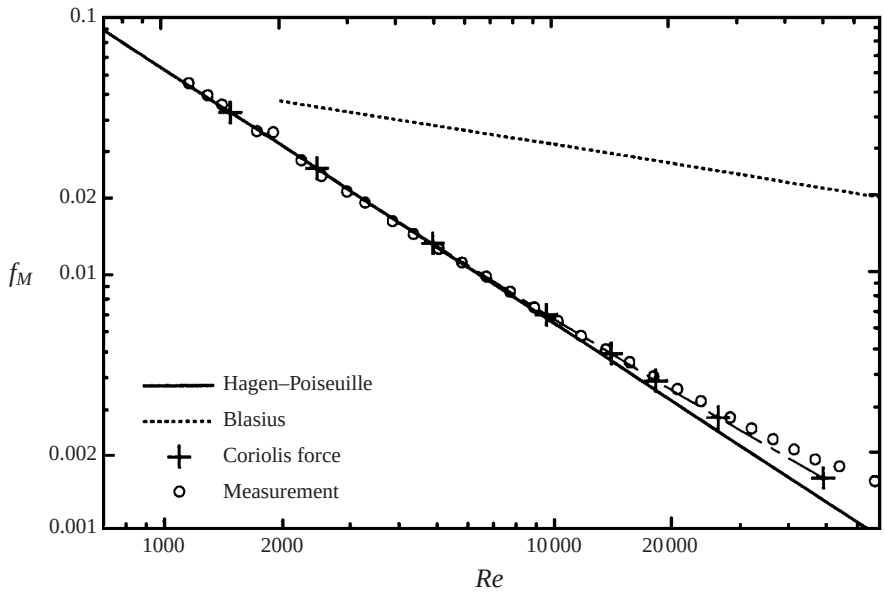

FIGURE 4. The Moody diagram for water as measured in the new pipe-flow facility. The points labelled 'Coriolis force' are results from numerical calculations accounting for the influence of the Earth's rotation on fully developed laminar pipe flow.

For fully developed laminar pipe flow, i.e. Hagen–Poiseuille flow, f_M varies with Re according to

$$f_M = 64/Re.$$

For turbulent pipe flow, the so-called Blasius law (Schlichting 1979, p. 597) applies when $Re < 10^{-5}$. It describes the relationship between f_M and Reynolds number Re according to

$$f_M = 0.3164\, Re^{-1/4}.$$

Both relationships are illustrated in figure 4 where we show the Moody diagram that we measure for our facility. It is clear that we can maintain laminar flow till Reynolds numbers $Re \simeq 60\,000$ which is thus by definition the natural transition number for our facility.

We have argued in § 2.1 that our facility allows fully developed laminar pipe flow only for $Re < 14\,300$. In figure 4, we observe that the measurements deviate from the fully developed Hagen–Poiseuille curve well before $Re = 14\,300$. The measurements are, however, close to the symbols labelled 'Coriolis force'. These points are obtained from a numerical solution of the complete nonlinear equations of motion for fully developed laminar pipe flow in which the influence of the Coriolis force caused by the earth's rotation has been included. Namely, though perhaps unexpectedly, it turns out that the laminar flow in our pipe-flow facility, is strongly influenced by this Coriolis force and for a detailed explanation of the background we refer to Draad & Nieuwstadt (1998).

Although the Moody diagram does not suggest a large deviation from fully developed conditions as result of this Coriolis force, the observed axial velocity profile is strongly distorted, as is illustrated figure 5. This figure shows also that at a Reynolds number of $Re > 18\,400$ the flow can no longer be considered as fully developed because the velocity profile becomes flat near the centre, an effect which is not found

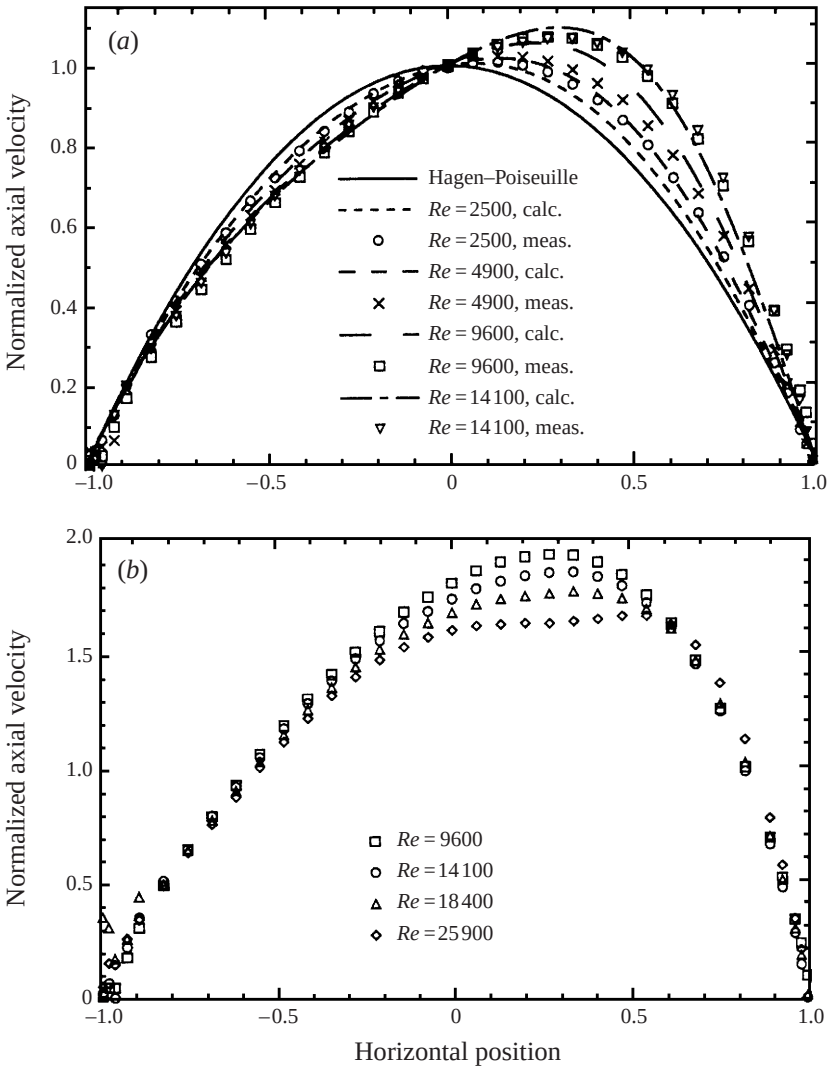

FIGURE 5. Axial velocity profiles in water in the horizontal plane. In (*a*) the velocity is normalized with the centreline velocity. The distortion of the axial velocity profile due to the Coriolis force increases with the Reynolds number; the solid line is the parabolic Poiseuille profile and the other lines represent the results of the numerical computations discussed in the text (Draad & Nieuwstadt 1998) In (*b*) the velocity is normalized with the bulk velocity. The present pipe-flow facility does not permit fully developed flow above Reynolds numbers of $Re = 14\,300$.

in our numerical computations of fully developed flow. The limited validity of fully developed flow conditions can be also discerned in figure 4 where for $Re \geqslant 14\,300$ the measurements deviate from the numerical solutions, labelled 'Coriolis force'.

2.3. *Disturbance mechanism*

Here, we discuss the mechanism by which we introduce a prescribed disturbance into the flow in order to trigger transition. In previous investigations injection by a single jet has been used to trigger a disturbance. However, such a disturbance is not divergence free and this may cause pressure perturbations at large distances from the injection point which may interfere with the pressure drop measurements. Instead, we

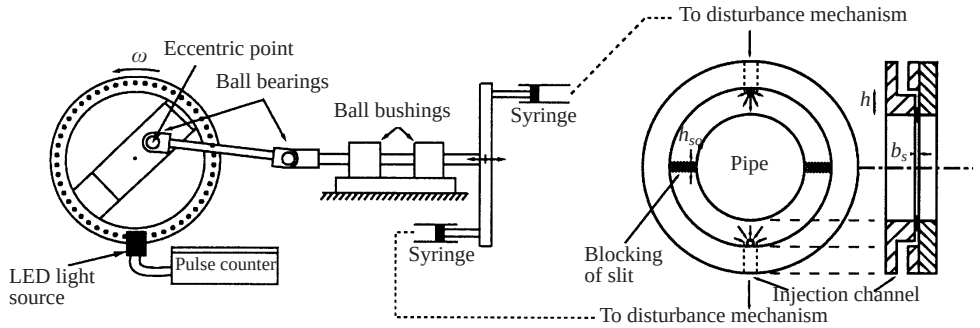

FIGURE 6. The set-up of the disturbance mechanism which is used to trigger transition; on the left we see the eccentric mechanism used to drive the two syringes which are used to produce a non-axisymmetric flow perturbation by periodically injecting and withdrawing fluid through the injection flange shown on the right; $b_s = 0.55$ mm, $h_s = 15.0$ mm, and $h_{so} = 3$ mm.

have applied a mechanism based on two oscillating syringes that move in opposite directions with respect to each other, as is shown in figure 6. This means that when one syringe is injecting, the other extracts fluid. The syringes are driven through an eccentric mounted on a wheel. The amplitude of the oscillation can be adjusted between 0 and 20 mm by changing the position of the eccentric point. The wheel on which the eccentric is mounted is driven by an electric motor the rotational speed of which can be varied on a continuous scale between 0 and 40 Hz. The frequency is measured using a pulse counter which has a resolution of 0.02 Hz.

We have used two types of commercially available syringes (BD Plastipak, 1 and 5 ml) with an internal diameter of 4.7 and 12.0 mm, respectively. These plastic syringes are placed inside Plexiglas holders to support the syringe wall and to prevent deformation. The soft rubber pistons that come with these syringes suffer so much elastic deformation at high frequencies that they no longer follow the displacement of the driving rod. Therefore, we have replaced them with plastic pistons. To prevent leakage we have applied quadrings (a special type of rubber ring with four-lobbed cross-section are much better suited for oscillating conditions and give less friction than e.g. O-rings) which fit in a groove in the pistons. The tubes which connect the syringes with the injection flange are made of transparent PVC. This material provides a stiff wall so that damping of the oscillating flow caused by flexibility of the tube wall is avoided. The inner diameter is 13 mm to minimize flow resistance which could lead to cavitation in the injection flange. The syringes, tubing and injection flange are all made of transparent material which allows visual inspection needed to detect any trapped air bubbles because a compressible air bubble would destroy the relationship between the amplitude of the syringes and the injection velocity.

The geometry of the injection flange is shown in figure 6. The fluid is injected/extracted perpendicularly to the pipe wall through two thin slits which measure about half the circumference. The construction has been made such that the suction/injection velocity is spread as evenly as possible over the entire circumference. In this way, the present disturbance is much more smooth compared to injection of a jet through a hole in the pipe wall. The simultaneous suction and injection, both with equal magnitude and along half the circumference of the pipe, implies that our disturbance has an azimuthal wavenumber equal to one (apart of course from higher harmonics). A similar suction/injection disturbance mechanism has been constructed

D_s (mm)	A (mm)	ΔV (mm^3)
4.7	1.00	17
4.7	2.00	35
4.7	4.99	87
4.7	10.01	174
12.0	3.01	339
12.0	4.99	565
12.0	10.01	1131

TABLE 1. Combinations of D_s, A and the corresponding displacement volume ΔV that are used in the stability measurements.

by Eliahou *et al.* (1998). In their case the mechanism consists of eight injection/suction slots which allows disturbances with an azimuthal wavenumber larger than one.

To characterize the disturbance, we employ its velocity and the frequency. As we do not know the precise azimuthal distribution of the suction/injection velocity, we define the disturbance velocity, v_i, as the injection velocity averaged over the slit area at the moment when the syringes reach their maximum velocity. The total injection+extraction area measures $O_{\text{ring}} = (\pi D - 2h_{so})\, b_s$, where b_s is the width of the slit and h_{so} is the length of the areas where the slit is blocked (see figure 6). The relationship between the maximum piston velocity $v_{p,max} = 2\pi f A$ with f the frequency and A the amplitude of the piston oscillation, and the disturbance velocity v_i is then governed by the ratio of the surface of the piston to that of the injection area ($O_{\text{ring}}/2$):

$$v_i = \frac{\frac{1}{4}\pi D_s^2}{\frac{1}{2}O_{ring}} v_{p,max} = 0.000\,190\,9 \times \tfrac{1}{4}\pi\, D_s^2\, A\, f = 0.000\,190\,9\, \Delta V\, f \tag{2.3}$$

where D_s is the inner diameter of the syringe. $\Delta V \equiv \pi A D_s^2/4$ is the displacement volume of the syringe in mm^3 (D_s and A have to be substituted in (2.3) in mm to give v_i in m s^{-1}).

Note that the disturbance velocity can be varied by changing either the ΔV or f. The frequency f can be adjusted by changing the rotational speed of the wheel which can be tuned very accurately (resolution 0.02 Hz). The displacement volume ΔV can be changed by a different mounting of the eccentric mechanism which determines the amplitude of the syringe piston. As a result, the ΔV takes discrete values, as given in table 1 while f can be varied continuously.

The experiments are now carried out by varying f at a given fixed value of ΔV and Re. From these data we can compute v_i so that the raw measurement data consist of combinations of v_i and f for various Reynolds numbers. The value of v_i at which transition is triggered, i.e. for all v_i below this value the flow remains laminar, is called the critical disturbance velocity and it is indicated as $v_{i,c}$.

2.4. *Transition detection*

To detect whether or not the disturbance has triggered transition, we monitor the centreline velocity with help of two LDV systems. Detection of transition by means of the centreline velocity is based on the fact that for laminar pipe flow the centreline velocity is substantially larger than for turbulent flow. In addition we measure the pressure drop over a length of 2.5 m. Transition to turbulence is easily detected

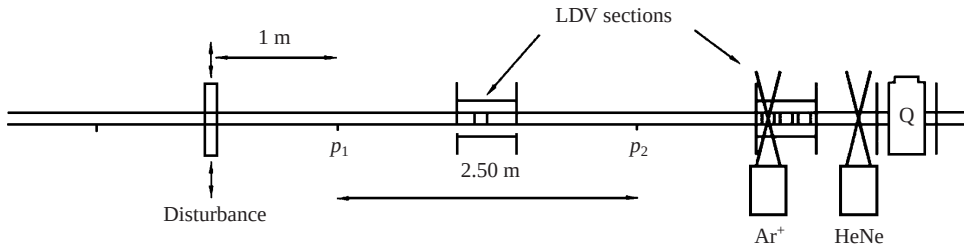

FIGURE 7. Configuration of the pipe segments and the measurement sections during the stability measurements. The squares inside the LDV-measurement sections having the size of the pipe diameter depict the location of the three thin sheets replacing the Plexiglas pipe wall; p_1 and p_2 indicate the location of the pressure holes. The magnetic inductive flow meter is labelled Q.

$z(p_1)$	$z(p_2)$	$z(\mathrm{Ar}^+)$	z(HeNe)
1.00 m	3.50 m	4.60 m	5.36 m
$25\,D$	$87.5\,D$	$115\,D$	$134\,D$

TABLE 2. Locations of the various components in the stability measurements. The axial positions are relative to the position of the disturbance placed 26.95 m downstream of the contraction. Values are given in physical length as well as number of pipe diameters.

with help of this (dimensionless) pressure drop since during transition the measured pressure gradient 'jumps' from the laminar Hagen–Poiseuille line to the turbulent Blasius line shown in figure 4.

The locations of these measurements are illustrated in figure 7. Their positions relative to the position of the disturbance mechanism, which is located at 26.95 m ($673.75\,D$) downstream of the contraction are given in table 2. This measurement configuration gives us four locations at which we can detect transition: the two LDV-locations and both pressure-hole locations.

For the pressure drop measurements we employ a membrane differential pressure transducer (Validyne Engineering Corp., type DP15-20) suited for pressure differences of 88 mm water full scale. The response is linear and pressure differences as small as 0.03 mm water can be detected. The pressure signal is rather noisy and therefore it is averaged over 30 s. The result is an accurate observation of the mean pressure drop (error less than 0.5%).

With the HeNe-laser system in combination with a frequency tracker we measure the velocity continuously. Due to the velocity range of this system we can only use it for flows with $Re \geqslant 7500$. We have also available an Argon-ion laser system together with a two-component full backscatter fibre-optic system manufactured by Dantec in combination with Burst Spectrum Analyzers (Dantec, type Enhanced 57N20 and 57N35). The fibre-optic system is placed on a computer controlled traversing mechanism such that velocity profiles can be measured fully automatically. In addition to average and r.m.s. velocities, the Dantec software can only display on line velocity histograms. This is adequate to detect transition at higher Reynolds numbers.

So, let us consider what happens if the disturbance velocity v_i raises above the critical value. Even though such a disturbance will by definition trigger transition somewhere downstream, v_i could be so close to the critical value that transition occurs downstream of the HeNe-LDV and according to our measurement system the flow would still be considered as laminar. When v_i is increased a little further, the

transition location will move upstream and transition may occur in between both LDV systems or even upstream of the Argon-LDV. Although the disturbance velocity can be adjusted very accurately, we found in most cases that transition is located either upstream or downstream of both LDVs and very rarely in between them. This is an indication that this far downstream of the disturbance position, the transition location is extremely sensitive to the value of v_i.

In most cases, however, it is possible to position the transition location in between the downstream pressure hole (p_2) and the Argon-LDV by carefully adjusting v_i. The distance between p_2 and the Argon-LDV is comparable to the distance between the two LDVs (27.5 D and 19 D respectively). Given this, we feel that for an accurate measurement of the critical disturbance velocity, the position of transition detection should be located at least 100 D downstream of the disturbance mechanism. Based on this choice, we use the LDVs rather than the pressure drop measurements to determine occurrence of transition. However, it is found that by using the pressure instead, only slightly larger values of the critical v_i are obtained than the values found from the LDV.

Increasing the disturbance velocity further by only a few percent will move the transition location close to the upstream pressure hole, so that both the LDVs and the pressure transducer detect turbulent flow.

Given the observed sensitivity of the transition location to the disturbance velocity, particularly for distances more than 100 D downstream of the position of the disturbance mechanism, we believe that the critical disturbance velocity v_i may be overestimated by less than 1 %.

2.5. *Non-dimensional quantities*

Now that we have defined the procedures to detect transition which allow accurate measurement of the critical disturbance velocity, $v_{i,c}$, let us consider the presentation of these measurements. In order to be able to compare our measurements with other experiments and theories, we need to transform these observations into appropriate dimensionless quantities.

In stability theory, the disturbance magnitude is commonly expressed as the ratio of the amplitude of the disturbance velocity and the velocity scale used in the definition of the Reynolds number. Following this convention we define the non-dimensional disturbance velocity as

$$v_i^* = v_i / \overline{W} \tag{2.4}$$

with $\overline{W}$ the bulk velocity as introduced before. For the non-dimensional critical disturbance velocity $v_{i,c}^*$ an equivalent definition is used.

The transformation of frequency into a dimensionless wavenumber as used in theory is more complicated. In linear stability theory, one usually adopts a disturbance varying according to $\sin[\alpha(z - c_r t)]$. Here, the wavenumber α is generally made dimensionless with the same length scale as is also used in the definition of Reynolds number, and the wave speed c_r with the same velocity scale. For our pipe flow these scales are D and $\overline{W}$, respectively. At fixed axial z-position the disturbance then varies in time according to

$$\sin(\alpha c_r t) = \sin(2\pi f t). \tag{2.5}$$

The wave speed c_r is not known in our experiments but in general c_r is of the order of $\overline{W}$. With this approximation the non-dimensional wave number becomes

$$\alpha^* = 2\pi f D / \overline{W}. \tag{2.6}$$

Finally, we note that if we plot $v_{i,c}^*$ as a function of α^* for several Re, we will find that all data points for a constant ΔV lie on a straight line crossing the origin. This follows directly from (2.3) together with the fact that both the disturbance velocity v_i and the wavenumber α are non-dimensionalized with $\overline{W}$.

Now that we have discussed all the tools to present the stability measurements, we first discuss the results for Newtonian fluids in the next section, which will also serve as a reference for the non-Newtonian stability measurements to be discussed in the section thereafter.

3. Newtonian stability measurements

In this section we present the results of the transition measurements for a Newtonian fluid (water) in terms the non-dimensional variables that we have discussed in the previous section. The detection of puffs structures which occur for $Re \leqslant 2700$ is rather difficult because these are characterized by only a gradual decrease in centreline velocity. At these low Reynolds numbers, the pressure drop measurement cannot be used to accurately detect transition. For these reasons we have restricted our main stability measurements to Reynolds numbers of 3000 up to $Re = 50\,000$. However, to give some indication of the behaviour of transition for $Re < 3000$ we will first discuss briefly some results that we have obtained at these low Reynolds numbers

3.1. *Observations at low Reynolds number*

For the low Reynolds numbers where puffs exist, we have recorded centreline-velocity time traces for Reynolds numbers 1800, 2000, 2200 and a few at 2500. For $Re = 1800$ the flow is found to decay to a laminar state. For $Re = 2000$ only a few puffs are observed whereas for $Re = 2200$ the number of puffs becomes much larger. For $Re = 2500$ the centreline velocity is close to the turbulent value most of the time and the shape of the time traces is in between that of puffs and slugs. Our measurements seem to support the existence of equilibrium puffs around $Re = 2200$ (Wygnanski *et al.* 1975).

Comparison of the critical parameters for the most efficient generation of puffs ($Re \leqslant 2700$) and of turbulent slugs at low Reynolds number values ($Re \approx 3000$) reveals that these are practically identical. This could suggest that puffs and turbulent slugs ($Re \geqslant 3000$) are produced as a result of a similar mechanism. This agrees with findings by Rubin *et al.* (1980) who show that merging of puffs leads to the formation of turbulent slugs. It would be interesting to investigate whether or not every turbulent slug originates from puffs. A method to do this would be by using PIV at several locations downstream of the disturbance injection location.

3.2. *Single and multiple transitions*

Let us now turn to our measurements for $Re > 3000$. The observations indicate that transition depends sensitively and also reproducibly on the frequency of the imposed disturbance. Although this may suggest that the transition from laminar to turbulent flow is determined primarily by the disturbance frequency, it will turn out that the frequency itself is not the principal parameter on which the transition depends. Namely, it should be kept in mind that our disturbance mechanism is based on an oscillation with a fixed displacement volume. Thus, by increasing the disturbance frequency, the disturbance *velocity* increases also according to (2.3). Therefore, in the following figures where we show pressure drop as a function of frequency, the dependence on frequency can be also interpreted as dependence on disturbance

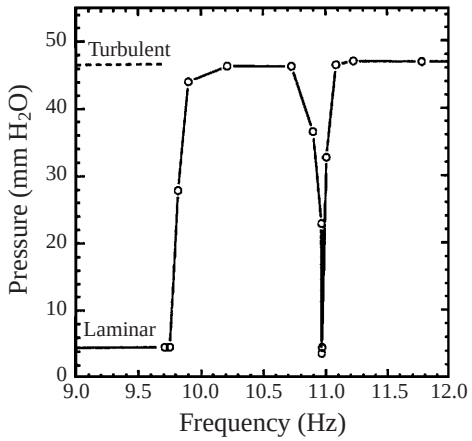

FIGURE 8. Measurement at $Re = 35\,000$, displacement volume $\Delta V = 35$ mm^3. Dotted line indicates full turbulent pressure drop.

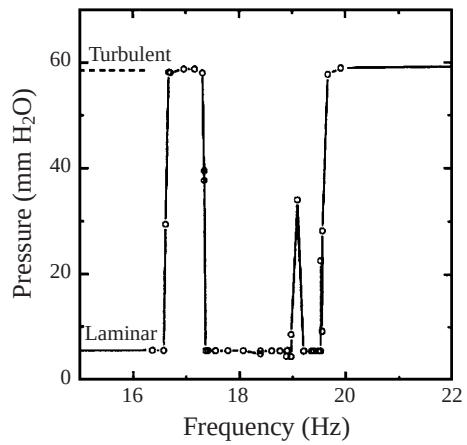

FIGURE 9. Measurement at $Re = 40\,000$, displacement volume $\Delta V = 17$ mm^3. Dotted line indicates full turbulent pressure drop.

velocity, where one can use (2.3) to transform the value of f into v_i. Nevertheless, we have chosen to present first results as a function of f, because that is how we have performed the experiment, i.e. changing f at fixed ΔV and Re.

In figure 8 we show the result of a single measurement at $Re = 35\,000$ and $\Delta V = 35$ mm^3. In this figure we have plotted the pressure drop between the two measurement locations mentioned in § 2.4 as a function of the frequency. Below $f \simeq 11$ Hz this is typical of most of our measurements: the pressure drop is equal to the laminar value until a critical frequency, or alternatively critical disturbance velocity $v_{i,c}$, is reached. Increasing the frequency further gives a transition which lies in between the two pressure holes and as a result the measured pressure drop lies in between the laminar and turbulent value. Eventually, the disturbance velocity is so large that transition to turbulence occurs within 1 m of the injection location resulting in a fully turbulent pressure drop.

However, figure 8 is peculiar in the sense that near $f \approx 11$ Hz increasing the frequency results in relaminarization of the flow and subsequently in a second transition.

Such measurements as presented in figure 8 are certainly not unique. In figure 9 we present the data obtained at a Reynolds number of $Re = 40\,000$ where we can discern turbulent regions for three separate ranges of the frequency, one of which does not seem to reach the full turbulent pressure drop.

To present the data in a more compact form we have reanalysed the data taken at several displacement volumes, frequencies, and Reynolds numbers in terms of the disturbance velocity as function of the Reynolds number for a given displacement volume. The results are plotted in figure 10(*a*)–10(*f*). The critical velocity is indicated in these figures by symbols connected by a line which separates the hatched 'laminar' area from the clear 'turbulent' area.

Figures 10(*a*) and 10(*b*) show clearly that apart from the 'standard†' laminar–turbulent transition, there seem to exist within the turbulent region several patches of laminar flow. The extremely narrow laminar region around 11 Hz found in figure 8 represents the 'nose' of the triangular shaped laminar region in figure 10(*b*), indicated by C. Although figures 10(*a*) and 10(*b*) appear to be similar at first sight, the behaviour at the smallest displacement volume, $\Delta V = 17$ mm^3, shows a much more complicated transition behaviour. For instance at Reynolds numbers around 30 000 and 40 000, small relaminarization and transition regions seem to exist as indicated by A and B respectively where the latter case has been also illustrated in figure 9. A much larger laminar area is formed for this value of ΔV for $Re > 32\,500$.

At a higher displacement volume, e.g. $\Delta V = 87$ mm^3 which is shown in figure 10(*c*), the stability diagram shows another behaviour, quite different from the results found at smaller ΔV values. In this case the critical disturbance velocity decreases drastically at Reynolds numbers just over $Re = 45\,720$. This behaviour has been checked by additional measurements for which we changed our measurement procedure. In this case, the frequency and consequently the disturbance velocity is kept constant and the flow rate, i.e. Reynolds number, is increased. The results obtained during these additional experiments are indicated in figure 10(*c*) by L (laminar) and T (turbulent). The results are in excellent agreement with the transition points found with the measurements obtained at constant Re values and varying disturbance frequencies (disturbance velocity). This fact, namely that the same result can be reproduced by two measuring procedures, gives us confidence that our observations are not in some way an artefact of the measurement procedure.

For displacement volumes $\Delta V = 173$ mm^3 and larger, shown in figures 10(*d*)–(*f*), no multiple transition points nor drastic changes in critical transition disturbance velocity have been found. For the three largest displacement volumes, shown in figure 10(*e*, *f*), the transition lines practically coincide. In other words, for these large values of ΔV the dependence on frequency is negligible and only the magnitude of the velocity disturbance matters.

In figures 10(*a*)–(*f*), an increase in disturbance velocity is linked to an increase in frequency following (2.3). The effect of solely a change in frequency at constant disturbance velocity, remains thus unrevealed. To show this dependency the data should be rearranged, e.g. by plotting the dimensionless disturbance velocity v_i^* against wavenumber α^* as defined by (2.6) for constant Re. The results are shown in figure 11 where figure 11(*b*) is an enlargement of the left-hand lower corner region of figure 11(*a*). Note that the measurement points in figure 11 are all located on seven straight lines (not shown) radially originating from the origin and repre-

† Standard should be interpreted here as the existence of a single (Re, v_i) point where the flow changes from laminar to turbulence.

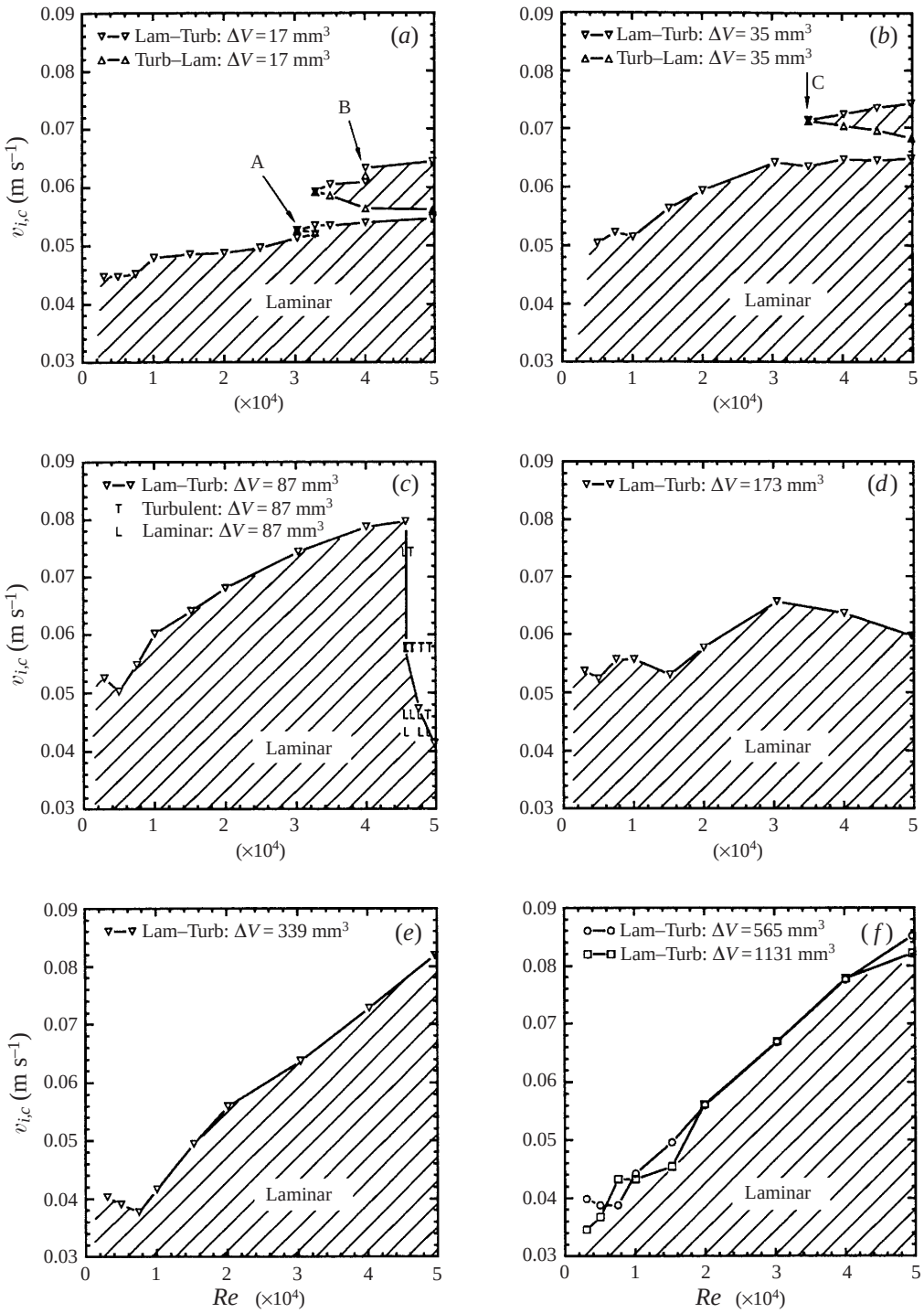

FIGURE 10. The disturbance velocity v_i versus Re for various displacement volumes; the symbols connected by a line indicate the critical disturbance velocity $v_{i,c}$ where transition from laminar to turbulent flow or vice versa is observed.

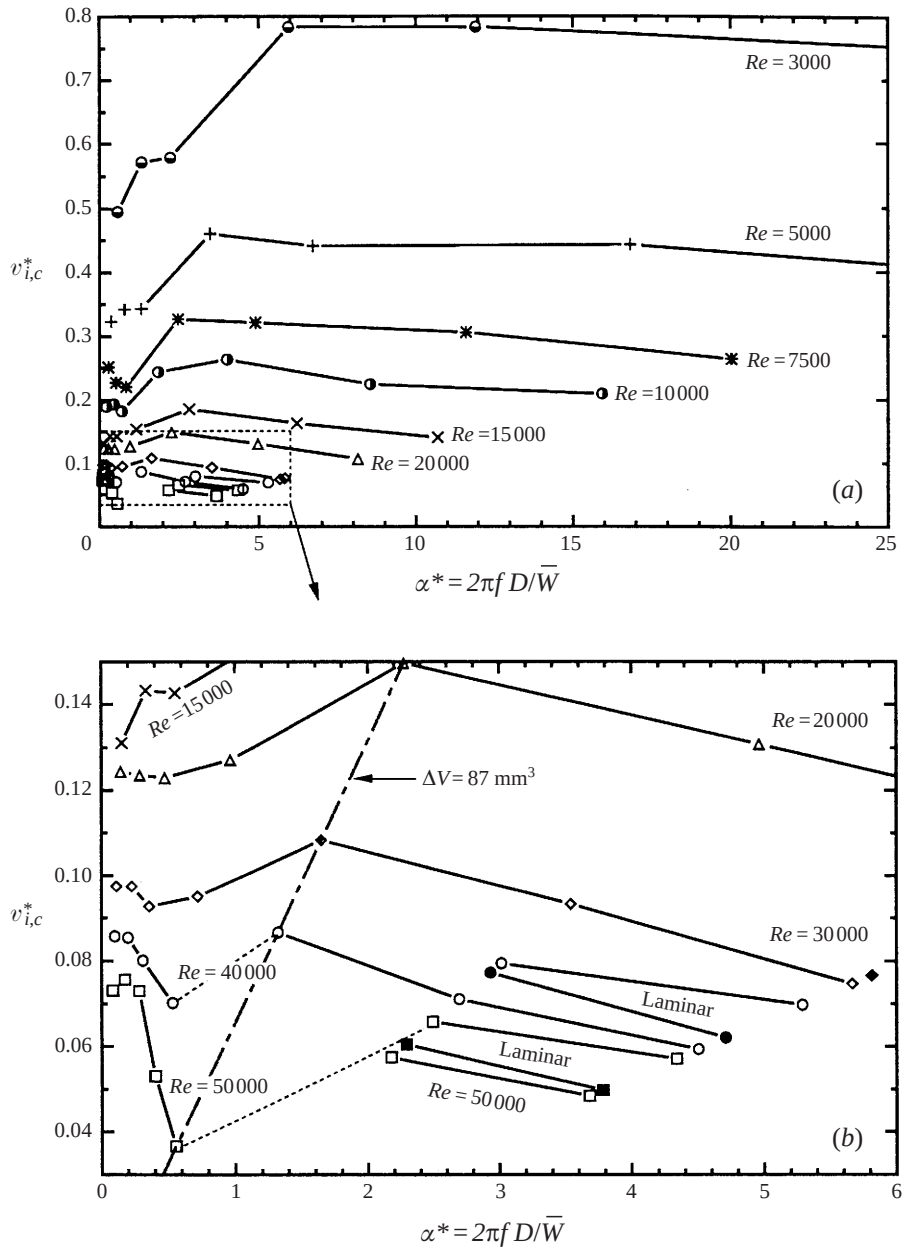

FIGURE 11. Critical non-dimensional disturbance velocity $v^*_{i,c}$ as a function of dimensionless wavenumber α^* for constant Reynolds number: (*b*) is an enlargement of figure (*a*) indicated by the dotted region. The open symbols indicated a transition point, i.e. a change from laminar to turbulent flow. The solid symbols indicate points where the flow relaminarizes if the disturbance velocity is increased at constant α^*. Each Reynolds number is represented by a unique symbol. If above a solid symbol no open symbol is present, then the two practically coincide. The indication 'laminar' marks the multiple transition region between the relaminarization and the second transition line. The lines for $Re \geqslant 40\,000$ for small α^* are not connected to those at large α^* due to the sensitivity of the flow around $\alpha^* \approx 1$.

senting the linear relation between $v^*_{i,c}$ and α^* discussed above in connection with (2.3).

We observe that the critical non-dimensional disturbance velocity $v^*_{i,c}$ decreases with increasing Reynolds number. This can be interpreted as the rather obvious result that at higher Reynolds numbers the flow is less stable. Usually, $v^*_{i,c}$ decreases with Re, but the *absolute* critical disturbance velocity $v_{i,c}$ may show a different behaviour and we found that $v_{i,c}$ increases with Re as shown in figure 10. Darbyshire & Mullin (1995) find a decrease of $v_{i,c}$ with Re. However, they used a single jet disturbance and in another experiment not discussed here, in which a single jet disturbance was employed, we also found a decrease with Re (Draad, Kuiken & Nieuwstadt 1995).

Above a dimensionless wavenumber $\alpha^* = 5$ the critical non-dimensional disturbance velocity $v^*_{i,c}$ seems only weakly dependent on α^*. At very small α^*, $v^*_{i,c}$ seems to be also constant but with a smaller value than at large α^*. Consequently, at intermediate values of α^*, $v^*_{i,c}$ depends both on α^* and Re.

As mentioned above, for low Re the level of $v^*_{i,c}$ at high values of α^* is in general larger than the value at low α^* and a change between these levels is found around $\alpha^* \simeq 1$. In contrast for $Re = 20\,000$ and higher, the values of $v^*_{i,c}$ at large α^* lie below those at small α^*. In addition, at these large Reynolds numbers, the flow seems to become extremely sensitive to disturbances with $\alpha^* \approx 1$, particularly at Reynolds numbers $Re \geqslant 40\,000$. (Although the measurements are not conclusive, and the large sensitivity to α^* is found in the range of approximately $0.6 \leqslant \alpha^* \leqslant 1.4$, we will use $\alpha^* \approx 1$ to indicate the region of this large sensitivity to α^*.) The measurements with $\Delta V = 87$ mm^3 illustrated in figure 10(*c*) are located precisely in this range and this explains the drastic fall in critical disturbance velocity found in this figure around $Re = 45\,720$. In fact, this shows the changeover at high Reynolds number from the small $v^*_{i,c}$ around $\alpha^* = 0.6$ to the multiple transition points for $\alpha^* > 2$. More measurements around this area are needed to describe the changeover more accurately. In analogy to the measurement procedure the results of which have been denoted by L and T in figure 10(*c*), variation of $v_{i,c}$ as a function of Re rather than the frequency f may be necessary here as the sensitivity to the frequency is too large.

The multiple transition regions found in figure 11(*b*) for $Re = 40\,000$ and $50\,000$ are located in the range $2 \leqslant \alpha^* \leqslant 6$. They are characterized by three transition lines: two laminar-turbulent transition lines called upper and lower which are depicted with open symbols and one turbulent–laminar transition (relaminarization) line indicated by the solid symbols. The solid symbol for $Re = 30\,000$ coincides with its upper laminar–turbulent transition point and is the representation of the small multiple transition area denoted A in figure 10(*a*). The relaminarization line and the upper laminar–turbulent transition line seem to approach each other when α^* is decreased thus bounding the extension of the multiple transition area. A similar trend can be discerned for the relaminarization line and the lower laminar–turbulent transition line with increasing α^*. More measurements are needed at intermediate values of ΔV to resolve the behaviour in this α^*-range at high Re.

Multiple transition points have also been found by Boere (1995), who performed experiments in the same experimental setup. At that time the natural transition Reynolds number was $Re \approx 30\,000$. After Boere finished his experiments, this natural transition Reynolds number was increased to more than 60 000 after some changes in the small settling chamber (see also § 2). Boere also found multiple transition points for $15\,000 \leqslant Re \leqslant 17\,000$ and $\alpha^* \approx 1.5$ using a displacement volume $\Delta V = 87$ mm^3 with a high sensitivity of the flow to disturbances around $\alpha^* \approx 1$. This could suggest that the phenomena found by Boere and ourselves are related. Perhaps the change in transition

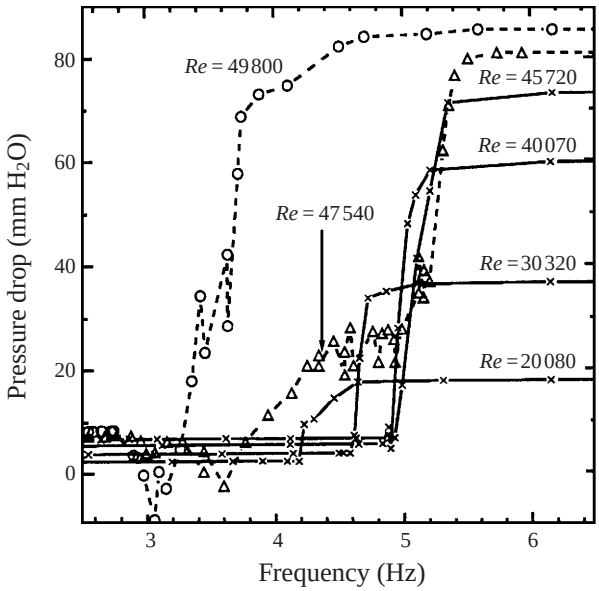

FIGURE 12. Pressure drop vs. frequency for various Reynolds numbers with $\Delta V = 87$ mm^3.

behaviour with an increase in α^* is linked to an interaction of small disturbances which are naturally present in the laminar flow and the artificial disturbances we added to the flow. For a comparison of the measurements by Boere with our stability results, the reader is referred to Draad (1996).

With respect to the high sensitivity of the flow for $Re \geqslant 40\,000$ and $\alpha^* \approx 1$, it is interesting to look again at the pressure drop as a function of frequency. In figure 12 we have plotted these variables at various values of Re for the case $\Delta V = 87$ mm^3. Up to $Re = 45\,720$ all curves exhibit a single sharp rise in pressure drop at a value of $f \simeq 5$. at which the pressure drop changes from the constant laminar value at the left to the turbulent value at the right of figure 12.

For the larger values of Re, i.e. $Re = 47\,540$ and $Re = 49\,800$, we notice at low values of f a decrease of the pressure drop below the laminar value. The pressure drops even becomes negative which implies that the downstream pressure is larger than the upstream pressure. This negative pressure drop, which is also measured for other values of Re, can be explained as follows. It occurs when the transition point is located near the most downstream pressure tap (p_2 in figure 7). During the transition, a redistribution of fluid from the centre of the pipe towards the wall takes place. The resulting change in total pressure near the wall causes an increase in measured pressure at p_2 that may exceed p_1, leading to a sub-laminar or even a negative pressure drop.

After this initial behaviour, the pressure drop for the case of $Re = 47\,540$ rises above the laminar value at low frequencies, i.e. $f < 5$, but does not reach the full turbulent pressure drop. Only at the transition frequency $f \simeq 5$ does the sharp rise in pressure drop to the full turbulent value occur. This behaviour might suggest that at approximately $f = 3$ Hz ($\alpha^* = 0.7$) a second disturbance mode is excited which at this Reynolds number of 47 540 has a much smaller growth rate than the mode which triggers turbulence at $f = 5$ Hz ($\alpha^* = 1.2$). This latter mode then takes over again at $f = 5$ Hz.

At still larger Reynolds numbers, e.g. $Re = 49\,800$, the growth rate of the second mode is large enough and the measured pressure drop rises at $f \simeq 3$ to the full turbulent pressure drop. The high sensitivity of the flow to disturbances with $\alpha^* \approx 1$ at $Re \geqslant 40\,000$ may thus be related to a competition between different instability modes. This fact and also the existence of multiple transition points for $Re \geqslant 30\,000$ and $\alpha^* \geqslant 2$ shows that the transition to turbulence in pipe flow is very complicated. Further research on this subject is needed to disclose the mechanisms behind this behaviour.

3.3. *Scaling of the critical velocity*

The way in which the stability measurements have been plotted in the previous subsection, i.e. $v_{i,c}^*$ vs. α^* at several Re, is well suited to show the high sensitivity of the flow to disturbances with $\alpha^* \approx 1$ and the location of the multiple transition points. It does not illustrate clearly, however, the dependence of $v_{i,c}^*$ on the Reynolds number at constant values of α^*. Such information is nevertheless very interesting as it would allow a comparison with existing stability theories. For instance, some nonlinear theories, e.g. those by Davey & Nguyen (1971), Smith & Bodonyi (1982) and Sen, Venkateswarlu & Maji (1985), predict that $v_{i,c}^*$ at constant α^* scales with Re to a certain power.

To extract this information from our stability measurements, we have used the following procedure. For constant values of α^* in figure 11, we apply a linear interpolation procedure to find the corresponding value of $v_{i,c}^*$ at a specific value of Re. For most Re values the change of $v_{i,c}^*$ with α^* is smooth so that linear interpolation will not introduce significant errors. For $\alpha^* = 2$ and $\alpha^* = 5$, extrapolation is needed for $Re \geqslant 40\,000$ and these points should thus be considered with care. Since we have found that the flow for $Re \geqslant 40\,000$ is very sensitive around $\alpha^* \approx 1$, no interpolation is allowed in this region. The results obtained from this interpolation procedure are collected in figure 13 where for various values of α^* the dependence of $v_{i,c}^*$ as function of Re is given.

A change in behaviour can be observed around $\alpha^* \leqslant 2$. For large α^*, i.e. 5 and 10, $v_{i,c}^*$ is practically independent of α^* and seems to vary according to Re^{-1}. This implies that the absolute critical disturbance velocity $v_{i,c}$ is independent of both α^* and $\overline{W}$. In other words, the Reynolds number $v_{i,c}D/\nu$ is constant and approximately equal to 2400.

For the very small wavenumbers $\alpha^* \leqslant 0.5$, $v_{i,c}^*$ is again practically independent of α^* but it now seems to vary according to $Re^{-2/3}$. This power is in agreement with the scaling rules found by Davey & Nguyen (1971) and Sen *et al.* (1985) for axisymmetric and non-axisymmetric disturbances respectively. In an appendix to the paper of Davey & Nguyen, Gill shows that a $Re^{-2/3}$ scaling rule is obtained when in the centre of the pipe the viscosity and the curvature of the velocity profile are used to construct a disturbance velocity scale. Davey & Nguyen also give a scaling rule for the length scale of the disturbance but no such information is available from our experiments. For intermediate values of $0.5 < \alpha^* < 2$, it seems that for low values of Re the scaling is according to $Re^{-2/3}$ while for larger values of Re the scaling seems again to follow the Re^{-1} behaviour.

The scaling of the critical relative disturbance velocity is nowhere near $Re^{-1/3}$ as proposed by Smith & Bodonyi (1982). This may be due to inapplicability of their theory or to the simple fact that the imposed disturbance in our case is not representative of the disturbance proposed by Smith & Bodonyi who introduce

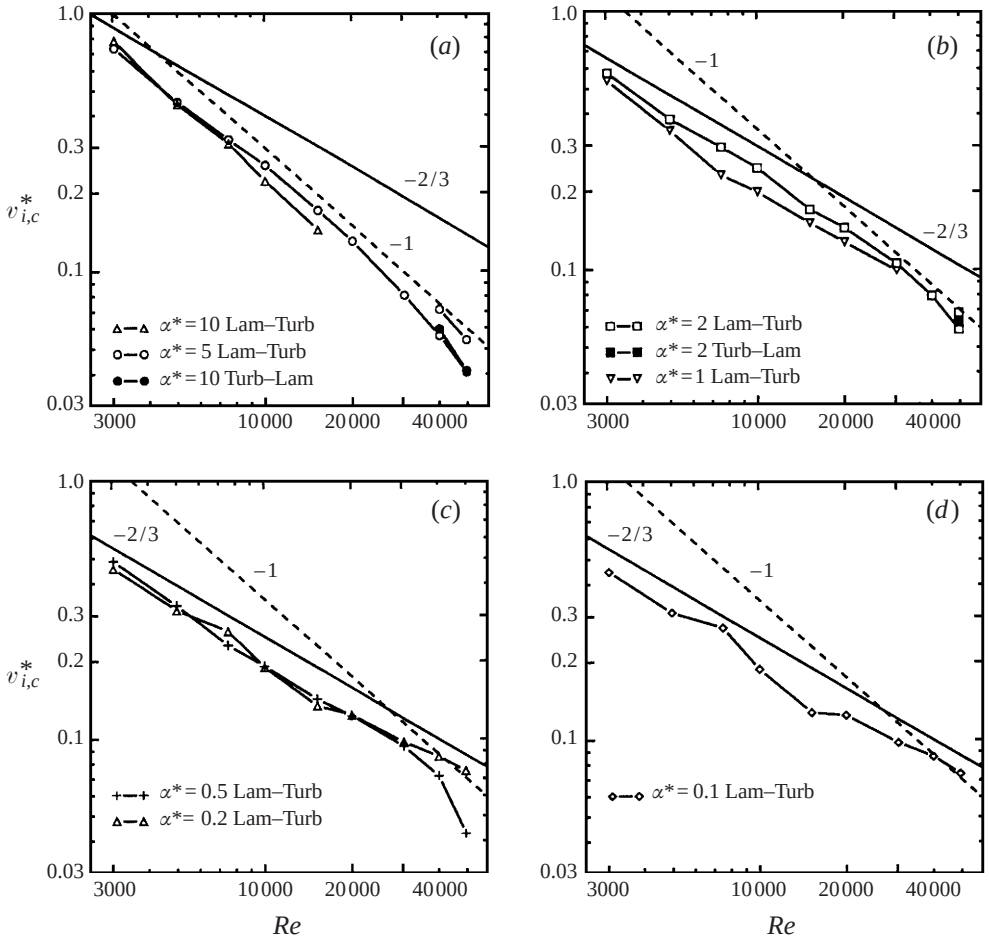

FIGURE 13. Critical relative disturbance velocity vs. Reynolds number for constant dimensionless wavenumbers $\alpha^* = 10, 5, 2, 1, 0.5, 0.2$, and 0.1. Note that the lines with slopes -1 and $-2/3$ have different origins in all four figures.

a disturbance which is sinusoidal in the tangential direction. Although the exact circumferential shape of our disturbance is not known, it has most probably no single sinusoidal dependence. For this, more injection points in the circumferential direction are needed.

Nevertheless, it is interesting to find that for small α^* the scaling of the critical disturbance velocity may have a link with theory and that for large α^*, the critical disturbance velocity is almost constant. This, together with the existence of multiple transition points, is more than sufficient reason to warrant further study both theoretically and experimentally.

4. Non-Newtonian stability

In this section, we will present our measurements on the stability of pipe flows for non-Newtonian fluids and compare the results with those for the Newtonian case presented above. To obtain a non-Newtonian fluid we dissolved polymers in water. Instead of mixing countless solutions of several concentrations of vari-

ous polymers, we have opted for a different approach: we have studied the transition behaviour of a polymer solution at three low concentrations (20, 30 and 40 p.p.m.) in combination with a variable salt concentration in the solvent. With the polymer that we use, this gives us the opportunity to change the polymer conformation between two extremes: fully coiled up at high salt concentrations and fully stretched at zero salt concentration. By studying the influence of the coil–stretch transformation on the stability of pipe flow of polymer solutions, we hope to reveal the key parameter(s) that govern(s) the transition to turbulence in these fluids.

To study the transition behaviour of the non-Newtonian fluids mentioned above, we perform two types of measurements. First, we measure the pressure drop as a function of the flow rate and plot the result as a friction factor versus a (viscosity corrected) Reynolds number, i.e. a Moody diagram. In these measurements turbulence can only develop by natural transition. Secondly, we determine the magnitude of the disturbance that is needed to trigger transition at various flow rates. These observations are transformed into a stability plot of the critical relative disturbance velocity $v_{i,c}^*$ versus non-dimensional wavenumber α^* for various Reynolds numbers. From these latter measurements we also extract the turbulent pressure drop and incorporate these points in the Moody diagram based on the first set of experiments without an imposed disturbance.

Let us first define some terms that we will use to describe our results. When, at the same Reynolds number, a larger critical relative disturbance velocity $v_{i,c}^*$, as defined according to (2.4), is found for the polymer solution than for water, we will speak of a *stabilizing* influence of the polymers. We stress, however, that this effect must be clearly distinguished from a *delay* in transition Reynolds number which is an increase of the minimum Reynolds number below which no transition can be initiated.

Furthermore, we have to take into account the non-Newtonian properties of the fluid, like a shear-rate-dependent viscosity, in order to make a correct comparison between stability measurements for polymer solutions and water at e.g. the same Reynolds number. The shear viscosity and also other fluid parameters such as the normal stress coefficients, are strongly related to the polymer conformation and we have argued above that this conformation can be influenced by the salt concentration. Therefore, we will first briefly discuss the effect of salt on the shear-rate-dependent viscosity and consequently on the pressure drop versus flow rate measurements in § 4.1. For a more detailed discussion on the subject we refer to Draad (1996). After correction for the shear-rate-dependent viscosity, the stability measurements for the polymer solutions will be compared to their Newtonian counterparts in § 4.2.

Before we start our presentation of the non-Newtonian data, we explain the notation that we will use for the concentration of the polymer solutions. To describe a polymer solution with a concentration of e.g. 30 p.p.m., a notation like $20 + 10$ p.p.m. may be used. This is to indicate that the 30 p.p.m. solution is obtained by adding 10 p.p.m. fresh polymer to an already used (and therefore somewhat degraded) polymer solution of 20 p.p.m. After performing stability measurements on the $20 + 10$ p.p.m. solution, we then may add another 10 p.p.m. of fresh polymer to obtain a 40 p.m.m. solution which is labelled as $20 + 10 + 10$ p.p.m. Although a totally fresh polymer solution of 40 p.p.m. is to be preferred over a $20 + 10 + 10$ p.p.m. solution, it is obviously much more work to produce such a fresh solution at a given concentration for each experiment and time was lacking for this. Nevertheless, we believe that the main conclusions of our stability experiments on polymers remain unaffected despite this procedure of adding fresh polymer to an already partly degraded solution.

4.1. *Properties of the non-Newtonian fluids*

Polymer degradation

In this subsection we consider various aspects of the fluids that we have used in our non-Newtonian experiments. The polymer that has been selected to make the solutions is a partially hydrolysed polyacrylamide (PAMH) with brand name Superfloc A-110 (Cytec Industries, formerly American Cyanamid), having a molecular weight of 6–8×10^6 g/mol. High-molecular-weight polymers are susceptible to mechanical and chemical degradation, i.e. the process of breaking the polymer chain by mechanical actions or chemical processes, respectively. Degradation results in a reduction of the molecular weight of the polymer, which in turn has a strong effect on its non-Newtonian properties. Since we use a recirculatory facility, special attention has been given to reduce the mechanical degradation as much as possible. The mechanical degradation will in principle determine the maximum measuring time, because severe degradation would lead to unacceptable changes in the measurement conditions. Let us therefore consider in some more detail the parts of our experimental facility which play a role in the process of mechanical degradation.

The pump is clearly a very important contributor to mechanical degradation. The severeness of degradation depends on the type of pump. Centrifugal pumps are very hostile to polymers whereas positive displacement pumps such as gear or progressive cavity pumps are known to be polymer friendly. A disadvantage of these latter pump types is that they give a pulsating flow. This is not acceptable for our case in view of the requirement that the flow should be disturbance free at the pipe entrance. Therefore, we have used a disc pump (Discflo Corporation, California USA) which is essentially a centrifugal pump with discs instead of fans. The advantage of this type of pump is that it combines relatively little degradation with a continuous flow. The application of a disc pump in combination with the large volume of the flow loop gives a reasonable time span of one to several days to perform measurements (additional information on the degradation experiments can be found in Toonder *et al.* 1995). Another contributor to mechanical degradation may be the screens in the settling chamber. We feel, however, that their contribution is negligible compared to the effect of the pump.

Polymers can be also subject to oxidative degradation by e.g. chlorine and peroxides. In our experiments with water we applied sodium hypochlorite to suppress the growth of algae but this cannot be used with PAMH-solutions as it strongly degrades the polymers. Also metal ions such as copper, iron and nickel enhance oxidative degradation.

Polyacrylamide solutions are non-corrosive to most common construction materials, but galvanized (zinc) or aluminium equipment should be avoided for corrosion reasons. It is therefore advisable to minimize the use of metals in components which have direct contact with the solution. In our case we have avoided all metals in our pipe facility as was already mentioned in § 2.1, with exception of the stainless steel fine screens in the settling chamber.

Influence of salt

As argued above, our choice of polymer is based on the fact that its conformation can be manipulated through a change of the salt concentration in the solution. In the absence of salt, the polymer has, on the average, a stretched conformation whereas the presence of salt forces the polymer to coil up. The coiling-up is stronger as the salt concentration increases. With respect to the type of salt it should be mentioned

Ion	Tap water	Softened water	Demineralized water	Demineralized water +0.001 M NaCl
Calcium Ca^{2+}	48	0.75	0.21	0.21
Magnesium Mg^{2+}	7.0	0.123	0.018	0.018
Sodium Na^{+}	34	94.4	1.19	1.19 + 23.6
Potassium K^{+}	5.0	0.6	2.8	2.8
Total divalent	55.0	0.873	0.228	0.228
Total monovalent	39.0	95.0	3.98	27.59

TABLE 3. Concentrations in mg l^{-1} of monovalent and divalent salts in tap water, softened water, demineralized water, and demineralized water with added salt. The listed values for demineralized water with 0.001 M NaCl are obtained by simply adding the 23.6 mg M Na^{+} corresponding to 0.001 M NaCl. Note that the softened water contains Na^{+} concentrations between that of 0.001 M and 0.01 M Na^{+}.

that the polymer that we use is more sensitive to divalent salts (e.g. magnesium Mg^{2+}, calcium Ca^{2+}) than to monovalent salts (e.g. sodium Na^{+}, potassium K^{+}) (Tam & Tiu 1990).

The influence of salt has been studied by performing stability experiments with help of softened water with 20 and 40 p.p.m. polymer, demineralized water with 20, 20 + 10 and 20 + 10 + 10 p.p.m. polymer and finally with the polymer solution of 20 + 10 + 10 p.p.m. in combination with three concentrations of salt. First, we have performed experiments using softened water which is obtained by running tap water through an ion-exchanger that replaces divalent salts with monovalent sodium salt. Since the concentration as well as the valency of the salts is important, fluid samples have been analysed and the measured salt concentrations for the various solutions are given in table 3. The values for tap water as supplied by the water company are added for comparison. From these data it follows that the process of softening water reduces the amounts of Mg^{2+} and Ca^{2+} to less than 1 mg l^{-1}. Furthermore, we have found that the increase of the viscosity due to polymers is larger in softened water than in tapwater. In other words, the PAMH polymers are stretched more in softened than in tapwater which is in agreement with the aforementioned sensitivity to the valency of the salts.

Secondly, we consider polymer solutions that contain even less salt than the softened water case. Ideally, distilled water should be used in this case. However, the system volume of the flow loop is 1.5 m^3 and to make distilled water in such large quantities is both time consuming and costly. Therefore, the best alternative is to use demineralized water which contains only very small amounts of salt as shown in table 3. The concentration of monovalent salt is seen to be much lower than in softened water, but also less divalent salt is present. With demineralized water as a solvent, we have performed experiments for several concentrations of the polymer.

For the operation of our magnetic flow meter which we use for the flow control, the fluid needs to be at least slightly conductive. The electric conductivity of demineralized water is very small. Nevertheless, our magnetic flow meter has been found to still function. For a laminar flow of demineralized water, the signal of the flow meter is stable but for turbulent flow large fluctuations in the signal occur. However, when averaged over half a minute, the signal produces an accurate flow-rate measurement.

Finally, to study the effect of salt on the flow behaviour in detail, three different salt concentrations have been considered. After the experiments with the 20+10+10 p.p.m.

A-110 solution in demineralized water, sodium chloride was added in three stages: 90 g, 810 g and 8100 g amounting to a total of 90 g, 900 g, and 9000 g respectively in 1.5 m^3 of solution. This corresponds to a concentration of 0.001 M, 0.01 M and 0.1 M NaCl respectively (1 M = 1 mol l^{-1}). For the softened water the concentration of monovalent salt is similar to that for a solution with between 0.001 M and 0.01 M NaCl and it will be interesting to see whether this similarity also applies to the flow behaviour.

Determination of fluid parameters

Let us now consider the effect of the polymers on the shear viscosity. For dilute polymer solutions, say with concentration of 40 p.p.m. and lower, an increase in viscosity and an effect of shear thinning are commonly disregarded. However, by measuring the viscosity with a Contraves Low Shear LS-40 concentric cylinder viscometer† we found even for a dilute polymer solution of 20 p.p.m. a measurable influence on the viscosity. At low shear rates in demineralized water the viscosity of this polymer solution was found to be almost 10 times that of water. For the case where the polymers are coiled up due to the presence of a large amount of salt, the viscosity of the 40 p.p.m. solution is closer to that of the solvent but still increased by 10%. The effect of low polymer concentrations on viscosity is confirmed by Vlassopoulos & Schowalter (1994) who found for a 2 p.p.m. polyacrylamide solution in distilled water (stretched polymers) a zero-shear-rate viscosity increase of 60% above the solvent viscosity. We must therefore conclude that a change of viscosity cannot be disregarded for dilute polymer solutions, certainly not for a stretched conformation but also not for coiled polymers.

In order to correct all non-Newtonian experiments for variable viscosity, we have measured the viscosity as a function of shear rate with the Contraves viscometer. From the measured data a viscosity function is determined which will be used to correct the Moody diagram and also to correct the stability measurements. As only shear viscosity is considered, we can model the effects of the polymers in terms of a generalized Newtonian fluid model. A widely used generalized Newtonian fluid model which captures a number of important parameters, is the four parameter Carreau model which describes the non-Newtonian viscosity η as a function of the shear rate $\dot{\gamma}$ (Bird, Armstrong & Hassager 1987*a*, p. 171) according to

$$\frac{\eta - \eta_\infty}{\eta_0 - \eta_\infty} = \left[1 + (\lambda\dot{\gamma})^2\right]^{(n-1)/2} \tag{4.1}$$

where η_0 is the zero-shear-rate viscosity, η_∞ the infinite-shear-rate viscosity, n the power-law exponent, and λ a time constant.

The Carreau model describes the transition from a zero-shear-rate plateau to a region following a power law with exponent n. A Newtonian fluid is represented by $n = 1$ and for a shear-thinning fluid $n < 1$. For the case of a dilute polymer solution the power-law region of the viscosity seems very often to level off at the higher shear rates. Our viscosity measurements indeed do show such a deviation of the power-law region at high shear rates. However, the measurements do not extend far enough in terms of $\dot{\gamma}$ and an accurate estimation of η_∞ is therefore impossible (although Kalashnikov (1994) used capillary viscometers and could obtain measurements in the η_∞-range). For this reason, we have set the value of η_∞ equal to the solvent viscosity

† The Contraves Low Shear LS-40 viscometer is especially designed for measuring low-viscosity fluids like water. According to specifications the LS-40 can measure the viscosity of water for shear rates ranging from 1 to 200 s^{-1} with an error of about 3%.

Concentration (p.p.m.)	Solvent (−)	Age (days)	η_0 (mPa s)	λ (s)	n (−)
40	Soft water	1	1.94 ± 0.02	1.16 ± 0.27	0.862 ± 0.006
20	Dem. water	1	9.58 ± 0.12	4.96 ± 0.03	0.612 ± 0.004
20		3	7.18 ± 0.07	2.81 ± 0.15	0.631 ± 0.004
20 + 10 + 10		1	$22.12^b \pm 0.38$	5.58 ± 0.54	0.643 ± 0.007
20 + 10 + 10	0.001 M NaCl	1[a]	$3.37^b \pm 0.02$	0.82 ± 0.08	0.772 ± 0.006
20 + 10 + 10	0.01 M NaCl	1[a]	$1.43^b \pm 0.01$	0.31 ± 0.09	0.877 ± 0.010
20 + 10 + 10	0.1 M NaCl	1[a]	1.02^b		1

[a]Viscosity measurements performed on 2 months old fluid samples.
[b]Moody diagram measurements after viscosity correction indicates an incorrect viscosity. For some cases a different value has been used in the viscosity correction procedure.

TABLE 4. Carreau model parameters according to (4.1) for some of the Superfloc A-110 polymer solutions used in the stability experiments. The η_∞ is set to the solvent viscosity value, thus giving $\eta_\infty = 0.904$ mPa s.

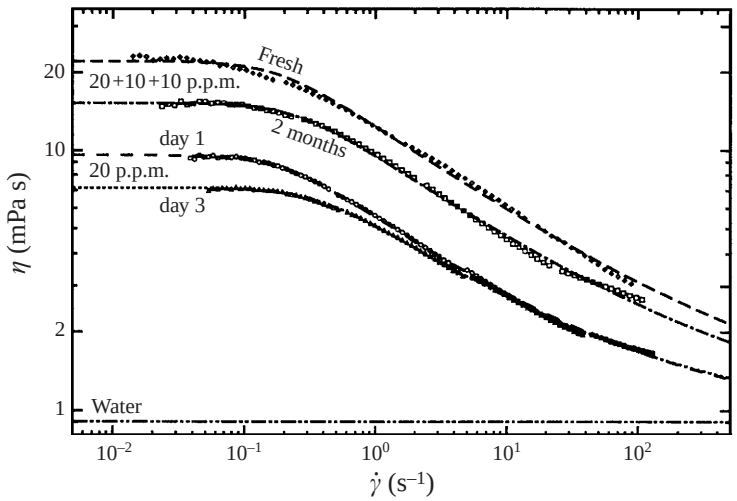

FIGURE 14. Non-Newtonian viscosity as a function of steady shear rate for several solutions of Superfloc A-110 in demineralized water. Measured using a Contraves Low-Shear LS-40.

value η_∞ (24.35 °C) = 0.904 mPa s which places in any case a lower bound on η_∞. For determination of the other parameters in (4.1), the software supplied with Gordon & Shaw (1994) has been used. The parameter values for the Carreau model found in this way are listed in table 4.

Several of the most representative results obtained in our viscosity measurements are illustrated in figures 14 and 15, where we plot the measured shear-rate-dependent viscosities (symbols) together with the fitted Carreau model (lines).

The results shown in table 4 and figures 14 and 15 give rise to the following remarks:

(i) On average, the viscosity data seem to be represented fairly well by the Carreau model. However, the value of η_∞ seems to be somewhat too small since for large shear rates, the measured viscosities are larger in most cases than the value predicted by

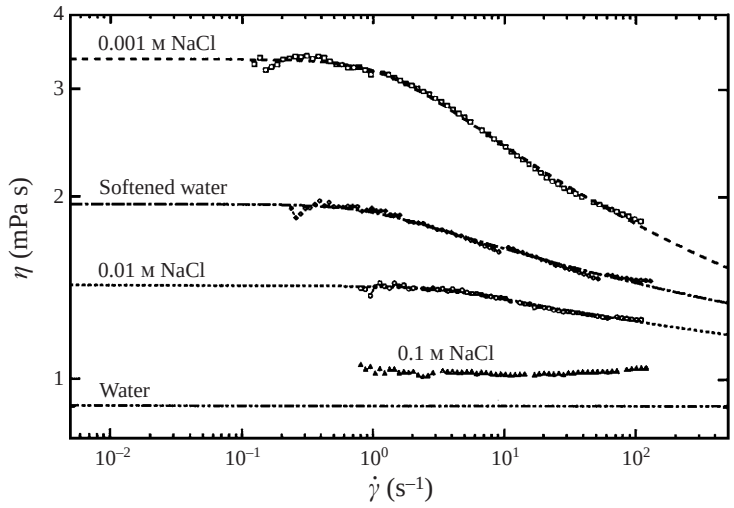

FIGURE 15. Non-Newtonian viscosity as a function of steady shear rate for 20 + 10 + 10 p.p.m. solutions of Superfloc A-110 in demineralized water after addition of various amounts of salt. The measurement of the 40 p.p.m. solution in softened water is added for comparison. Measured using a Contraves Low-Shear LS-40.

the Carreau model. A larger value of η_∞ than that of the solvent would have resulted in a better fit. Nevertheless, for the purpose of transforming our measurement data, the Carreau model using the solvent value for η_∞ is quite suitable since the stability measurements are not located in the high-shear-rate range.

(ii) The dissolving of small amounts of polymer in demineralized water results in a spectacular increase in viscosity. The time constant increases to approximately $\lambda = 5$ s. The shear thinning is significant with $n \approx 0.6$. This value is remarkably close to the value $n = 2/3$ found for rigid dumbbells from kinetic theory (Bird *et al.* 1987*b*, p. 123). This could be an indication that the stretched polymers show rod-like behaviour.

(iii) From the data given in figure 14, we see that mechanical degradation of the 20 p.p.m. A-110 solution in demineralized water mainly affects the viscosity primarily at low shear rates. Also, chemical degradation with time (aging) occurs as is shown by the difference between the measurement of the fresh 20 + 10 + 10 p.p.m. solution and that measured two months later. Thus to obtain the correct shear-rate-dependent viscosity, the rheometric measurements should be performed immediately before and/or after the transition experiments.

(iv) Adding a small amount of salt results in a dramatic decrease of the viscosity as shown in figure 15. The reason for this is the coiling up of the polymer caused by the presence of salt. Addition of 0.001 M NaCl reduces η_0 to approximately 1/6 its value in demineralized water. The time constant becomes $\lambda = 0.82$ s, which is even smaller than found with softened water as solvent but it should be mentioned that the uncertainty in the time constant is quite large. Adding ten times more sodium chloride reduces the viscosity to values that are smaller than those for softened water. This is in agreement with the salt content given in table 3. Finally, for 0.1 M NaCl, the viscosity is reduced to a value only 10% above that of water and hardly any shear thinning remains.

Viscosity-corrected Reynolds number

We have observed that for dilute polymer solutions, in particular when the polymers have a stretched conformation, the viscosity is considerably larger than that of the solvent. In addition a shear-thinning behaviour has been found. In a laminar pipe flow the shear rate is different at every radial location in the pipe and depends also on the flow rate. So, which viscosity should one use in the calculation of the Reynolds number? Use of the solvent viscosity gives unsatisfactory results. This follows from figure 16(*a*) where the results obtained with the solvent viscosity are denoted as 'raw data'. As a result of the large increase in viscosity, the data are shifted strongly to the right of the Hagen–Poiseuille line and are moreover not parallel to this line.

As an initial step toward a definition of a modified Reynolds number, we first consider a power-law fluid. Although this model does not describe the shear-rate-dependent viscosity in our case as well as the Carreau model, with help of this model we can derive explicit relationships which are impossible to obtain with the Carreau model. Furthermore, the power-law model captures the power-law region of the viscosity function that is also present in the Carreau model.

The (empirical) power-law model describes the non-Newtonian viscosity as a function of shear rate according to $\eta = K\dot{\gamma}^{n-1}$. With this expression the following relationship for the friction factor for laminar pipe flow can be derived (Bird *et al.* 1987*a*, p. 177):

$$f_M = \frac{\Delta p\, D}{\frac{1}{2}\rho\, \overline{W}^2} = \frac{64\,\eta_w}{\rho\, \overline{W}\, D}\,\frac{3n+1}{4n} = \frac{64}{Re_n}, \tag{4.2}$$

where η_w is the viscosity at the wall. Re_n is introduced as a modified Reynolds number which is defined as (Metzner & Reed 1955)

$$Re_n = \frac{\rho\, \overline{W}^{2-n} D^n 2^{3-n}}{K\,(3+1/n)^n} \tag{4.3}$$

and which leads, as follows from (4.2), to the well known relationship between the friction factor and Re_n according to the Hagen–Poiseuille relation for a Newtonian fluid.

However, based on (4.2) we can consider an alternative: namely, the use of a Reynolds number in which the viscosity is taken equal to its value at the wall. The relationship between this Reynolds number, denoted as Re_w, and Re_n is

$$Re_w \equiv \frac{\rho\, \overline{W}\, D}{\eta_w} = \frac{3n+1}{4n}\, Re_n. \tag{4.4}$$

The advantage of using Re_w instead of Re_n lies in the fact that it can be used for any viscosity model both in laminar and in turbulent flows. Re_w requires only the viscosity at the wall, the determination of which will be discussed later. A disadvantage is that the use of Re_w rather than Re_n in the Moody diagram will result in an overestimation of the Reynolds number by a factor $\frac{1}{4}(3+1/n)$. As for our polymer solutions $n \geqslant 0.612$ the error introduced by the use of Re_w will be at most 16%. For the Carreau model and for the range of parameters in this model that are representative of our data, it is smaller than 8% for $Re_w > 2000$. This result seems quite acceptable and given all the practical advantages, we have decided to use Re_w in all our plots, both for the Moody diagram and the stability measurements.

To calculate Re_w it remains to determine η_w. In our case the following procedure has been used:

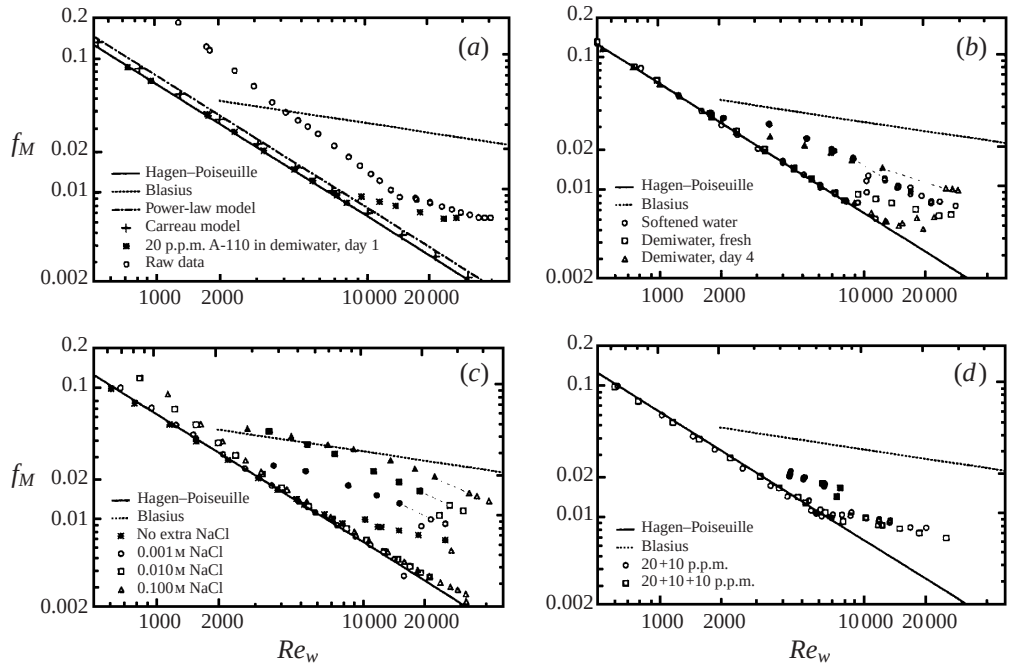

FIGURE 16. Moody diagrams for several solutions of Superfloc A-110 using the Reynolds number based on the viscosity at the wall, Re_w. The solid symbols represent the measurements where transition is triggered by adding a disturbance and the open symbols denote measurements without any artificial disturbance added; the dashed lines connecting adjacent points with and without an imposed disturbance are given to guide the eye; (*a*) The measurements (raw and corrected) for the fresh 20 p.p.m. Superfloc A-110 solution in demineralized water compared to the theoretical relationships for the power-law model and the Carreau model; (*b*) several 20 p.p.m. solutions in softened water and demineralized water (fresh and degraded); (*c*) the influence of sodium chloride salt on the flow behaviour of the $20 + 10 + 10$ p.p.m. solution in demineralized water; (*d*) the fresh $20 + 10$ p.p.m. and the $20 + 10 + 10$ p.p.m. solutions in demineralized water.

(*a*) the Carreau model parameters for the fluid are determined from the viscometer measurements;

(*b*) the measured pressure drop is transformed into a wall shear stress using $\tau_w = \Delta p\, D/(4L)$;

(*c*) the relation between the shear stress τ and the shear rate $\dot{\gamma} = \partial w/\partial r$ is formally given by $\tau \equiv \eta(\dot{\gamma})\dot{\gamma}$ where in our case $\eta(\dot{\gamma})$ is given by the Carreau model obtained in step (*a*). So, from the τ_w obtained in step (*b*), the values of η_w and $\dot{\gamma}_w$ can be determined by iteration and with this Re_w can be calculated.

The procedure described above must be carried out for all data points.

Using this procedure for the fresh 20 p.p.m. A-110 polymer solution, we obtain the corrected Moody diagram as shown in figure 16(*a*). For comparison we show in the same figure the Hagen–Poiseuille line as well as the result for a power-law fluid with $n = 0.612$ and the Carreau model ($\lambda = 4.96$ and $n = 0.612$). Rather surprisingly, the measurements fit closer to the Hagen–Poiseuille line than to the results obtained with the Carreau model. This seems to be the general trend for most of our data. Although the difference between the Hagen-Poiseuille line and the line for which Re_w is based on the Carreau model is small, i.e. smaller than 8% for the solutions that we used, it is nevertheless noticeable.

A possible explanation for the deviation of the measurements from the line computed with the Carreau model is that this model does not give a perfect fit to the viscosity data. We have tried to identify sources of discrepancy. As an example we may mention the small jumps that are found in some of the viscosity measurements. They are caused by the switching between ranges of the torque transducer of the viscometer. Recalibration of the transducer has almost eliminated these discontinuities. Another source of discrepancy is the value of η_∞ which is somewhat too small and this leads to small deviations between the viscometer measurements and the Carreau-model fit. Finally, a discrepancy between the viscosity-corrected data and the theoretical prediction may also result from the fact that the fluid samples which have been taken from the vessel are not entirely representative for the fluid in the pipe. Taking fluid samples at the end of the pipe through a small hole in the pipe wall would probably have been a better option.

Non-triggered Moody diagrams

We have determined the Moody diagram for several other flow cases than the 20 p.p.m. solution and the results are presented in figures 16(*b*)–16(*d*) (the solid symbols represent measurements where transition is triggered by imposing a disturbance and which will be discussed in the next subsection). These data lead to several interesting observations which we discuss in turn below.

(i) As already mentioned, almost all laminar data coincide practically with the Hagen–Poiseuille line. As the viscosity functions of the various polymer solutions are quite different, we feel that our choice of the use of Re_w is supported by this result. In contrast, the measurements for 0.01 M and 0.1 M NaCl, shown in figure 16(*c*), exhibit a deviation from the Hagen–Poiseuille line, particularly at the lower values of Re_w. A possible explanation for this deviation is that the fluid samples for the viscosity measurements have been taken from the reservoir too early at a time when the mixing was still incomplete.

(ii) The Moody diagrams for the non-Newtonian fluids show a different behaviour with respect to natural transition when compared to that of a Newtonian fluid. Whereas the natural transition Reynolds number for Newtonian fluids has been found to be larger than $Re = 60\,000$, the non-Newtonian polymer solutions have natural transition Reynolds numbers in the range of $8000 \leqslant Re \leqslant 30\,000$. Natural transition Reynolds numbers of $Re \approx 8000$ are shown in figure 16(*b*,*d*) for polymer solutions with various concentrations of Superfloc A-110 in demineralized water, where the polymers have a stretched conformation. Natural transition Reynolds numbers of $Re \approx 30\,000$ are found for the $20+10+10$ p.p.m. polymer solution in the presence of the highest salt concentration that we studied, i.e. 0.1 M NaCl, as shown in figure 16(*c*).

(iii) All polymer solutions show drag reduction, i.e. the turbulent f_M-curve lies below the Blasius line. This means that for turbulent flow, at the same Reynolds number, the friction factor is smaller for the polymer solutions than for water.

(iv) In demineralized water the polymers have, on average, a stretched conformation. This results in type-B drag reduction (see Virk & Wagger 1990) in which case the turbulent data start to deviate from the laminar line by just gradually bending away from it, as shown in figure 16(*d*). The characteristic jump in friction factor, normally associated with transition of Newtonian fluid and also with a type-A drag reduction fluid, related to coiled polymers, has vanished. An example of this latter behaviour can be seen in figure 16(*c*) where the jump in the transition reappears when salt

has been added to the polymer solution, which, as we have argued above, forces the polymers to a coiled conformation.

(v) When the fluids are aged, the natural transition Reynolds number increases and the amount of drag reduction becomes smaller, as follows from figure 16(*b*). This decrease in drag reduction with circulation time over a short period of several days is commonly attributed to mechanical degradation, i.e. the breaking of polymer molecules due to mechanical forces. For mechanically degraded polymer solutions in demineralized water, the jump in friction factor when going through transition to turbulence, which was almost absent for fresh polymer solutions, appears again.

(vi) By adding 10 p.p.m. of fresh polymer to the degraded 20 p.p.m. solution in demineralized water after 5 days (the degraded solution after 4 days is shown in figure 16(*b*), we obtain the $20 + 10$ p.p.m. solution displayed in figure 16(*d*). From this figure it is clear that adding fresh polymer practically restores the turbulent flow behaviour to that of the fresh 20 p.p.m. polymer solution. The viscosity is increased but this is concealed in the use of Re_w. The $20 + 10 + 10$ p.p.m. solution is obtained by adding 10 p.p.m. of fresh polymer to a slightly degraded $20 + 10$ p.p.m. solution.

(vii) A spectacular change in flow behaviour can be seen after the addition of sodium hypochlorite to the fluid (not shown). This results in the restoration of the Newtonian flow behaviour: a natural transition Reynolds number of 60 000 is again obtained and the viscosity is only 5% above that of water. Presumably, the polymers are completely degraded due to chemical processes. Therefore, no sodium hypochlorite can be added to the water, resulting in a limited measuring time of less than one week due to the growth of algae, particularly at the high water temperatures that we encountered during our experiments.

Triggered transition in Moody diagram

In figures 16(*b*)–16(*d*) we have also plotted the measurements for triggered turbulence as solid symbols. In comparison to the non-triggered data, shown as open symbols, several interesting results can be noted.

Let us first consider the phenomenon of drag reduction by polymers. It has been recently argued (Toonder *et al.* 1997) that drag reduction is primarily due to a purely viscous anisotropic stress introduced by extended or stretched polymers. Thus, the so-called 'onset' of drag reduction, i.e. the value of the wall shear stress above which drag reduction begins, is likely to be related to turbulence becoming strong enough to stretch the polymers from a coiled to an extended conformation, as was already suggested by Virk & Wagger (1990). Above this onset point, the increase in drag reduction with an increase in Reynolds number can then be explained as a greater proportion of the polymers being stretched by the turbulent flow and thus becoming effective as drag reducers. With this explanation in mind we now consider figure 16(*c*) where we present the influence on the drag due to the adding of salt which as mentioned before promotes the coiling of the polymers. Clearly, the 0.1 M solution shows a higher onset Reynolds number than the 0.01 M solution, whereas the 0.001 solution displays no onset behaviour but drag reduction as soon as the flow becomes turbulent. These results are in accordance with the coil–stretch transformation hypothesis for the onset Reynolds number.

Comparing the degraded solution in demineralized water with the solution in softened water as shown in figure 16(*b*), indicates that the results for demineralized water display slightly more drag reduction for $Re \leqslant 10\,000$ whereas the reverse is true above this Reynolds number. This result may be explained as follows. In softened water, the polymers are much less extended than in demineralized water. For low

Reynolds numbers, the turbulence is not strong enough to stretch the polymers in the softened water solution, thus resulting in less drag reduction than the degraded demineralized water solution. When, at higher Reynolds numbers the turbulence is strong enough to stretch the polymers, the undegraded solution in softened water shows more drag reduction since in this case its polymers are longer and therefore more effective than those in the degraded demineralized water solution.

For the fresh polymer solutions in demineralized water as shown in figure 16(*d*), the triggered points show a rather unexpected behaviour. Namely, the measured friction factors for the triggered transition (solid symbols) are much higher than what would follow from extrapolation of the turbulent data obtained without any added disturbances (open symbols). A discussion of these results is deferred to the next section.

From the Moody-diagram results discussed above, it is clear that non-Newtonian flow behaviour is rather complicated and susceptible to various influences. Although we can make a fair prediction of the qualitative effect of the non-Newtonian fluid properties on the flow behaviour, a quantitative prediction is still impossible. This remains one of the most important challenges in non-Newtonian fluid mechanics.

4.2. *Stability measurements*

In this section, we discuss the results of the forced stability experiments for the non-Newtonian fluids and compare the data with the results obtained for the Newtonian fluids of § 3.

We carried out measurements for certain flow rates which for a Newtonian fluid would correspond to following rounded-off values for Re: $Re = 3000$, 5000, 7500 and 10 000. However, we have argued that Re_w should be used in this case to characterize the flow. Remember that in the calculation of Re_w the viscosity at the wall is used. This results for the case of constant Re in Re_w values that vary with each solution. For example, the flow rate corresponding to $Re = 7500$ for water, gives $Re_w = 4400$ for the 40 p.p.m solution in softened water and $Re_w = 2600$ for the $20 + 10$ p.p.m. solution in demineralized water, respectively. This complicates the comparison but rather than interpolating the data to lines for the same value of Re_w for all fluids, we have chosen to present the stability data without such data manipulation. In the stability diagrams, the quantities plotted along both axes, i.e. the critical relative disturbance velocity $v^*_{i,c}$ and the dimensionless wavenumber α^*, are both unaffected by the viscosity. Thus, the non-Newtonian viscosity correction appears only in the value for the Reynolds number Re_w.

Before discussing the stability measurements, in particular those of the fresh polymer solutions in demineralized water, some further discussion on the background of these measurements is needed. As discussed in § 2.4, transition is detected by pressure-drop observations over a pipe section of 2.5 m starting 1 m downstream of the disturbance mechanism and also by using LDV techniques. As illustrated in figure 7 both the Ar-ion and the HeNe LDV are located further downstream than the pressure drop measurement. As a consequence, the LDV equipment can detect transition slightly earlier than the pressure-drop measurement.

For Newtonian fluids, a strong increase in pressure drop and strong fall in centreline velocity are clear indicators of transition. The same characteristics can be also used to identify transition in the polymer solutions made with softened water and the degraded polymer solutions in demineralized water. However, for fresh polymer solutions in demineralized water, we have found in figure 16(*d*) that no jump in pressure drop occurs when going through transition. This effectively eliminates the pressure drop as

an indicator for transition and leaves us only with LDV measurements. Unfortunately, the fresh polymer solutions in demineralized water do also not show a clear drop in centreline velocity which would indicate turbulence. Although shear-thinning fluids have a laminar velocity profile which is somewhat blunter than a parabola, the shear-thinning effect for the fluids used here ($n \leqslant 0.61$) is not strong enough to explain the absence of the drop in centreline velocity. Thus, it is likely that in this case analogously to the pressure drop data the entire velocity profiles changes continuously from the laminar to the turbulent profile. This is not unreasonable since the velocity gradient near the wall is coupled to the wall shear stress in the viscous sublayer and the wall shear stress is linearly related to the pressure drop. Therefore, we propose here to use the turbulence intensity as the only reliable indication for transition in fresh polymer solutions in demineralized water.

Let us present another argument to apply turbulence intensity as transition indicator. As we will see later, a delay of transition for the polymer solutions is found. In combination with the low natural transition Reynolds number, we are left in this case with only a small *Re*-range in which the transition can be triggered. From Newtonian stability experiments, we know that just above the lowest possible transition Reynolds number so called turbulent puffs appear. Puffs, in particular when their number is small, cause only a small decrease in average velocity. Such a small decrease in average velocity is also what we found for transition with the fresh polymer solutions in demineralized water, but more study, e.g. by measuring time traces, is required to confirm the existence of puffs in non-Newtonian fluids. The turbulence intensity, however, increases from the laminar value of 1–2% to typically 2.5–3%. This in combination with a slight decrease in the average centreline velocity can be used as a clear indication that the flow has become (at least partly) turbulent.

In the stability diagrams to be shown in the following subsection, we plot the critical relative disturbance velocity $v^*_{i,c}$ as a function of dimensionless wavenumber α^* for various Re_w values. The diagrams, which are based on a complete measuring program, have been obtained for the 20 p.p.m. and 40 p.p.m. solutions in softened water (not shown here) and for the mechanically degraded 20 p.p.m. as well as for the 20 + 10 p.p.m. solution in demineralized water. For all other solutions, we carried out only a limited measuring program, i.e. only one or two displacement volumes ΔV were considered. The reasons for this are related to time constraints as well as mechanical degradation.

We first discuss the $v^*_{i,c}$ vs. α^* stability diagrams based on the full measuring program for the two solutions, mentioned above, separately. Then, we will compare the stability of other solutions where the measurements were performed for only one or two displacement volumes.

Stability results for mechanically degraded solution in demineralized water

Due to the problems with the transition indicators described above, only one displacement volume could be studied for the 20 p.p.m. solution in demineralized water, the results of which will be shown later in figure 20. By the time the problem was recognized, the solution had degraded. Before adding an extra 10 p.p.m. of fresh polymer, the stability diagram of the degraded 20 p.p.m. solution was measured during the 4th and 5th day and the results are shown in figure 17.

When comparing the results for this mechanically degraded 20 p.p.m. solution in demineralized water with those for the Newtonian fluid shown in figure 11, we find that the effect of the polymers is on average to stabilize the flow, i.e. the critical disturbance velocity, $v^*_{i,c}$, is higher than the equivalent value for the Newtonian fluid.

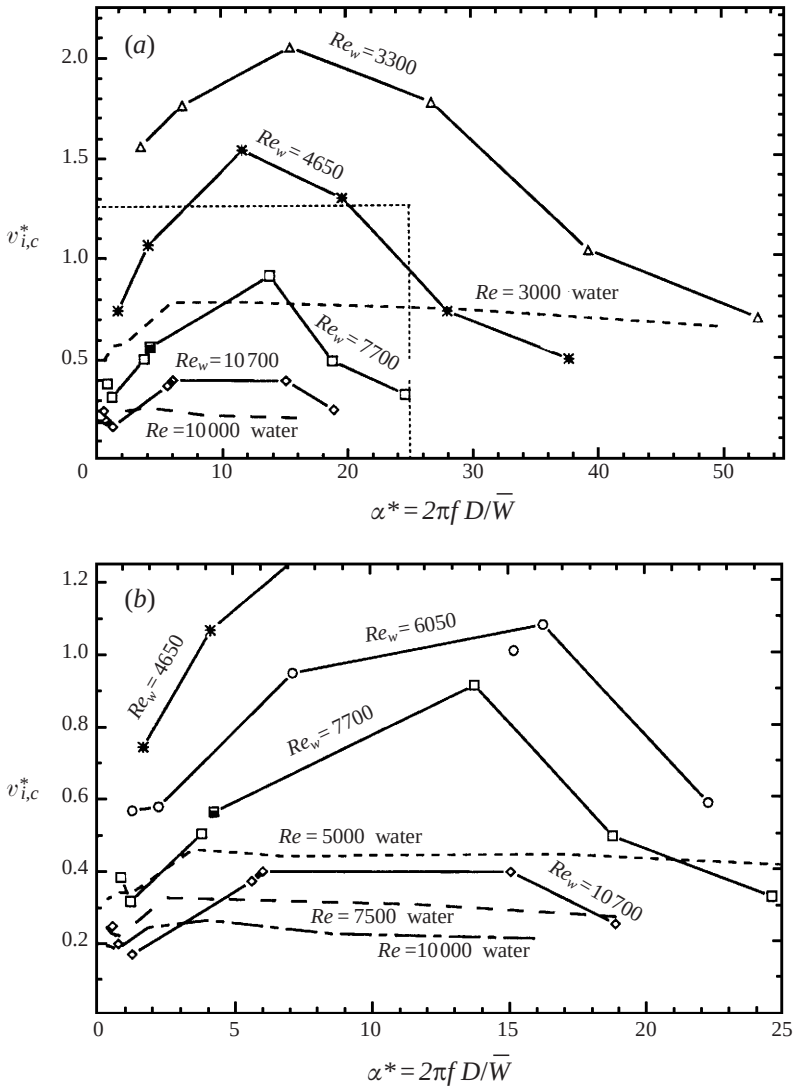

FIGURE 17. Critical relative disturbance velocity $v^*_{i,c}$ as a function of dimensionless wave number α^* for various Reynolds numbers for a mechanically degraded 20 p.p.m. Superfloc A-110 solution in demineralized water water after circulation for 4 to 5 days; (*b*) is an enlargement of (*a*). The solid symbols indicate points where the flow relaminarizes if $v^*_{i,c}$ is increased (multiple transition points). For reasons of comparison, the results for water are plotted using dotted lines.

The largest stabilizing effect is found around α^* values from 10 to 20. Above and below these values the critical relative disturbance velocities fall sharply and approach those for water. For $Re_w \approx 10\,000$ and at $\alpha^* \approx 1.5$, the polymer solution is even slightly less stable than water. Multiple transition points appear around $\alpha^* \approx 5$, which is close to those found for Newtonian fluids. Also, for $Re_w = 7700$ and $Re_w = 10\,700$, an enhanced sensitivity of the flow to disturbances with $\alpha^* \approx 1$ seems to emerge, similar to what we have found for Newtonian fluids for $Re \geqslant 30\,000$.

Based on the results obtained so far, we conclude that for a mechanically degraded polymer solution of Superfloc A-110, in general larger $v^*_{i,c}$ values are found than in

water, i.e. we have *stabilization*. However, it should be emphasized that despite this stabilizing effect, the flow can still be triggered to undergo transition to turbulence at $Re_w = 3300$ which is very close to the Newtonian value of $Re \approx 3000$. Therefore, no *delay* in transition is found for this mechanically degraded solution, i.e. the minimum transition Reynolds number has not changed with respect to the Newtonian value.

Stability results for fresh solution in demineralized water

Adding 10 p.p.m. fresh polymer solution to a degraded 20 p.p.m. solution in demineralized water (denoted by $20 + 10$ p.p.m.) restores the smooth natural transition as found for the fresh 20 p.p.m. polymer solution (see figure 16*d*). The resulting stability diagram in dimensionless form for forced disturbances is shown in figure 18.

The two thick irregular lines in figure 18 indicate the maximum disturbance velocity that could be achieved with the present disturbance mechanism but at which the flow remained nevertheless laminar. These lines depend on the following criteria. The maximum α^* that can be obtained is given by the maximum frequency of $f = 39$ Hz. This leads to a maximum α^* value of 57 and 39 for $Re_w = 2600$ and $Re_w = 3600$, respectively. For smaller α^*, the thick lines roughly indicate settings where cavitation is initiated in the injection flange or where severe mechanical oscillations arose due to a large out-of-balance weight for eccentric positions of 5 mm.

Even for the maximum disturbance velocities at $Re_w = 2600$ and 3600 given by the thick lines, no turbulent flow could be triggered. Only at $Re_w = 4100$ and larger can the flow be forced to undergo transition. In other words, we have a delay in transition for the $20 + 10$ p.p.m. solution in demineralized water till $Re \approx 4000$. This value is fairly close to Reynolds number at which the extrapolated turbulent line intersects with the laminar line for the data shown in figure 16(*d*).

At Reynolds numbers for which turbulent flow can be triggered, the polymers strongly stabilize the flow; critical relative disturbance velocities are more than twice as large as those for water. However, for $\alpha^* < 5$ the stabilizing effect seems to decrease strongly as the Reynolds number is increased. For $Re > 6000$ natural transition sets in, thereby limiting a triggered transition to the range $4000 \leqslant Re \leqslant 6000$.

With respect to the Reynolds number value to which the transition is delayed, it is interesting to look at the triggered transition points represented by the solid symbols in figure 16(*d*). The triggered transition points represent the maximum pressure drop that was found for a $\Delta V, Re$-combination as a function of disturbance frequency. These data seem to suggest by extrapolation to the laminar limit that the minimum transition Reynolds number is smaller than $Re_w \simeq 4000$.

For the degraded and salty solutions, we did find a plateau region in the turbulent pressure drop for large disturbance frequencies. For the fresh demineralized water solutions this was not the case. The measured pressure drop increases with increasing frequency (and thus increasing disturbance velocity). Very often, it reaches a maximum and decreases again after the frequency is increased further, in particular for Reynolds numbers close to the minimum transition Reynolds number (below which no transition could be triggered).

All this may indicate that the flow is still developing and may even decay back to a laminar flow when given enough time. Proof that developing lengths can be increased for non-Newtonian fluids in comparison with Newtonian fluids is reported by Bewersdorff (1991). He used surfactant solutions which form rod-like micelles and found that as much as 280 diameters are needed to generate a fully developed turbulent pipe flow for these fluids, which is much larger than the $40\,D$–$100\,D$ recommended for Newtonian fluids.

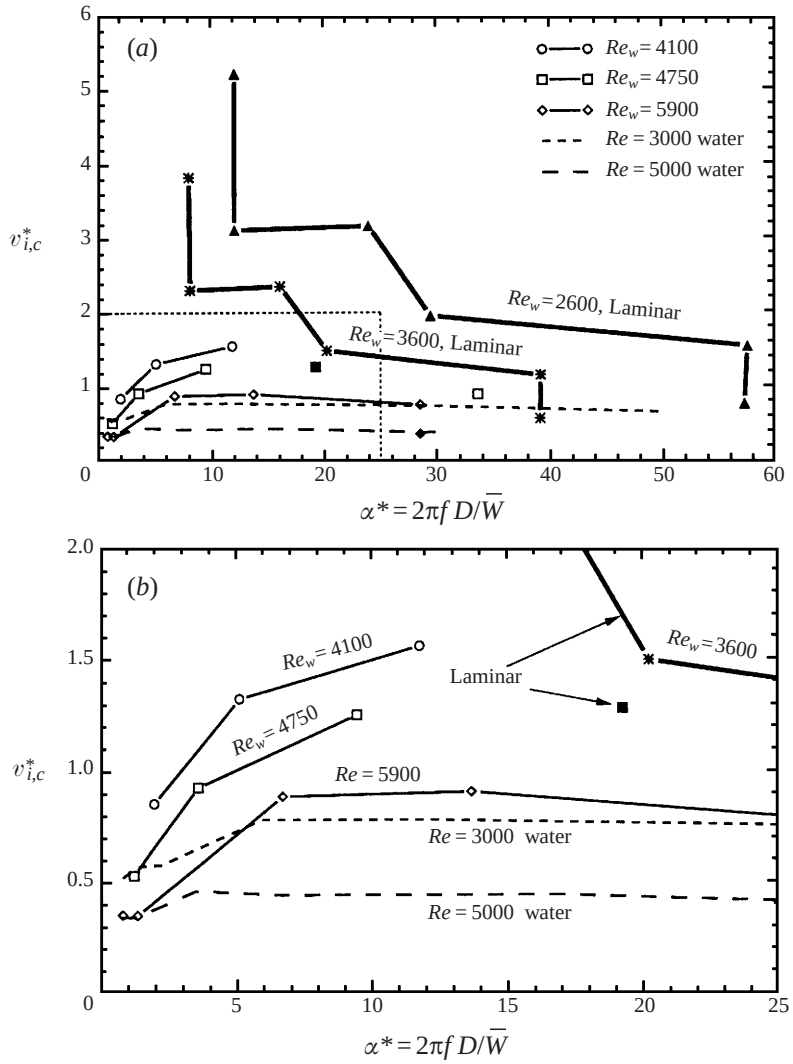

FIGURE 18. Critical relative disturbance velocity $v^*_{i,c}$ as a function of dimensionless wavenumber α^* for various Reynolds numbers for a 20 + 10 p.p.m. Superfloc A-110 solution in demineralized water water. The thick lines with the solid symbols indicate the maximum disturbance that could be imposed and where the flow still remains laminar; (*b*) is an enlargement of figure (*a*). No multiple transition points are present. For reasons of comparison, the results for water are plotted using dotted lines.

Thus, if the triggered transition points (solid symbols) in figure 16(*d*) indeed represent turbulent flows that are decaying, we may not use them to estimate the minimum transition Reynolds numbers. This possibly brings the minimum transition Reynolds number closer to that of the intersection between the laminar and the turbulent lines. Further research is necessary to establish this.

The stability diagram for the 20 + 10 p.p.m. solution in demineralized water thus leads to the conclusion that the Reynolds number below which no transition to turbulence could be found is increased to a value of $Re_w \approx 4000$. This value seems to be independent of α^*, i.e. the Reynolds number to which the transition is delayed can

be determined without measuring a large range of frequencies. Thus, if this is true in general, we can determine the Reynolds number below which no turbulence can be triggered by performing a stability measurement for only one ΔV. If finding the minimum transition Reynolds number is the only objective, a measurement procedure using only one ΔV would save a large amount of time and it would also reduce the problem of mechanical degradation.

Stability results obtained for constant ΔV

With the final remark of the previous subsection in mind, we decided to perform stability measurements for the $20 + 10 + 10$ p.p.m. solution in demineralized water for only two displacement volumes, i.e. $\Delta V = 565$ mm^3 and $\Delta V = 174$ mm^3. For the $20 + 10 + 10$ p.p.m. solutions in combination with salt, we performed stability measurements for $\Delta V = 565$ mm^3 only. The choice of these displacement volumes is based on the fact that we can achieve the largest $v_{i,c}^*$ with these values for ΔV (see figure 18, where for a line with constant Re_w the point with the largest ΔV is the point to the left with the smallest α^*). Precisely for these small values of α^*, small $v_{i,c}^*$ values are found. This combination of a small $v_{i,c}^*$ needed to trigger transition to turbulence and the capability of disturbing the flow with very large v_i ensures that, if transition can be triggered, we are also likely to be able to introduce a disturbance of sufficient magnitude such that transition will occur.

The stability measurements for $\Delta V = 565$ mm^3 and $\Delta V = 174$ mm^3 are given in figures 19 and 20 respectively. Comparing figures 19(*a*) and 20(*a*), we see that the stability measurements for the 20 p.p.m. and 40 p.p.m. solutions in softened water almost coincide. An exception is the multiple transition area found in figure 20(*a*). For $Re_w > 10\,700$, we find from figure 20(*a*) that the mechanically degraded 20 p.p.m. solution in demineralized water is less stable than for water. On the other hand, for low Re_w this solution shows a strong stabilizing effect, but no delay in transition is found. However, the measurements must be extended to lower Re_w to allow an accurate estimate of the minimum transition Reynolds number. Particularly, the measurements for the 20 p.p.m. solution in softened water show no large increase in $v_{i,c}^*$ when Re_w is reduced to $Re_w = 2100$. Such an increase for Re close to the minimum transition Reynolds number in Newtonian fluids has been reported by Darbyshire & Mullin (1995). This could even suggest that for the polymer solutions in softened water, the minimum transition Reynolds number is smaller than the value for water, which implies a transition enhancement. Further research is needed to disclose such behaviour.

Figures 19(*b*) and 20(*b*) show that the fresh polymer solutions in demineralized water lead to a *delay* in transition. Particularly, the $20+10+10$ p.p.m. solution shows a delay in transition to $Re_w \approx 5000$. This is very close to the intersection of the turbulent data with the Hagen–Poiseuille line shown in figure 16(*d*). Thus, it seems that this intersection is a good estimate of the minimum critical Reynolds number for solutions in which the polymers have a stretched conformation. Above a Reynolds number Re_w of 4000 the fresh $20 + 10$ p.p.m. and $20 + 10 + 10$ p.p.m. solutions in figure 19(*b*) display lower $v_{i,c}^*$ values than the mechanically degraded 20 p.p.m. solution. This could be related to the lower natural transition Reynolds number for fresh polymer solutions.

The values of $v_{i,c}^*$ for the fresh polymer solutions for which no transition could be triggered are very close to the $v_{i,c}^*$ values of the mechanically degraded solution in the measurements for $\Delta V = 174$ mm^3, as shown in figure 20(*c*). For $\Delta V = 565$ mm^3,

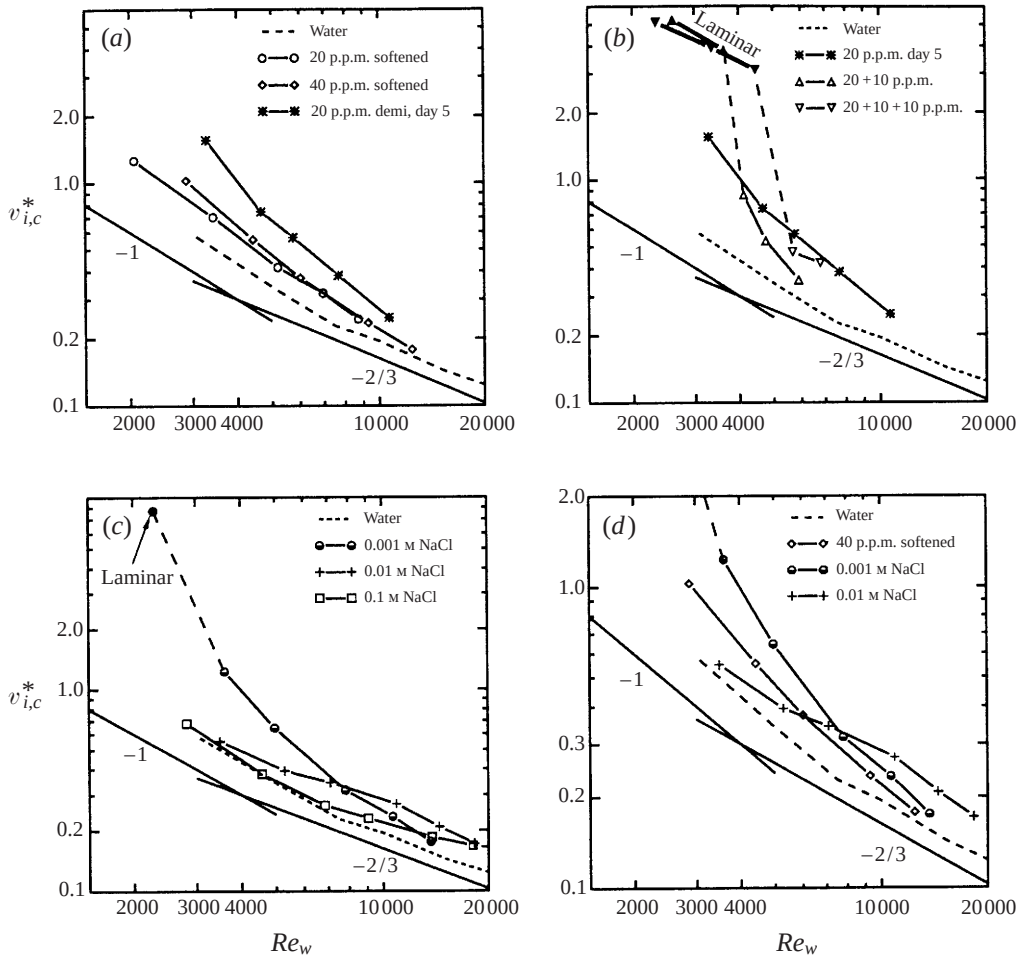

FIGURE 19. Critical relative disturbance velocity vs. Reynolds number for Superfloc A-110 solutions in various solvents for displacement volume $\Delta V = 565$ mm^3. No multiple transition points are present and all solid symbols indicate points where no transition could be triggered at the maximum disturbance velocity available, and are labelled 'laminar'.

i.e. figure 19(*b*), this difference is much larger, which gives more confidence in the observed delay in transition.

The stability measurements for the $20 + 10 + 10$ p.p.m. solutions with added salt illustrated in figures 19(*c*) and 19(*d*) show that for the 0.001 M solution no transition could be triggered for $Re_w = 2300$. It also follows that for $Re_w \leqslant 7500$, the 0.001 M solution is more stable than the two other solutions containing more salt. The 0.1 M solution contains more salt than softened tap water and its stability behaviour is very close to that of water, so that the polymers are apparently strongly coiled and have no stabilizing effect. For $Re_w \geqslant 7000$, the 0.1 M solution is more stable than water and the stabilization increases with the Reynolds number. Perhaps, the much higher shear rates at these high Reynolds numbers cause the polymers to partly stretch and slightly stabilize the fluid. Surprisingly, the 0.001 M solution (in which the polymers are certainly stretched to some extent) is less stable than the 0.01 M solution at high Reynolds numbers. This may be a result of the lower natural transition Reynolds

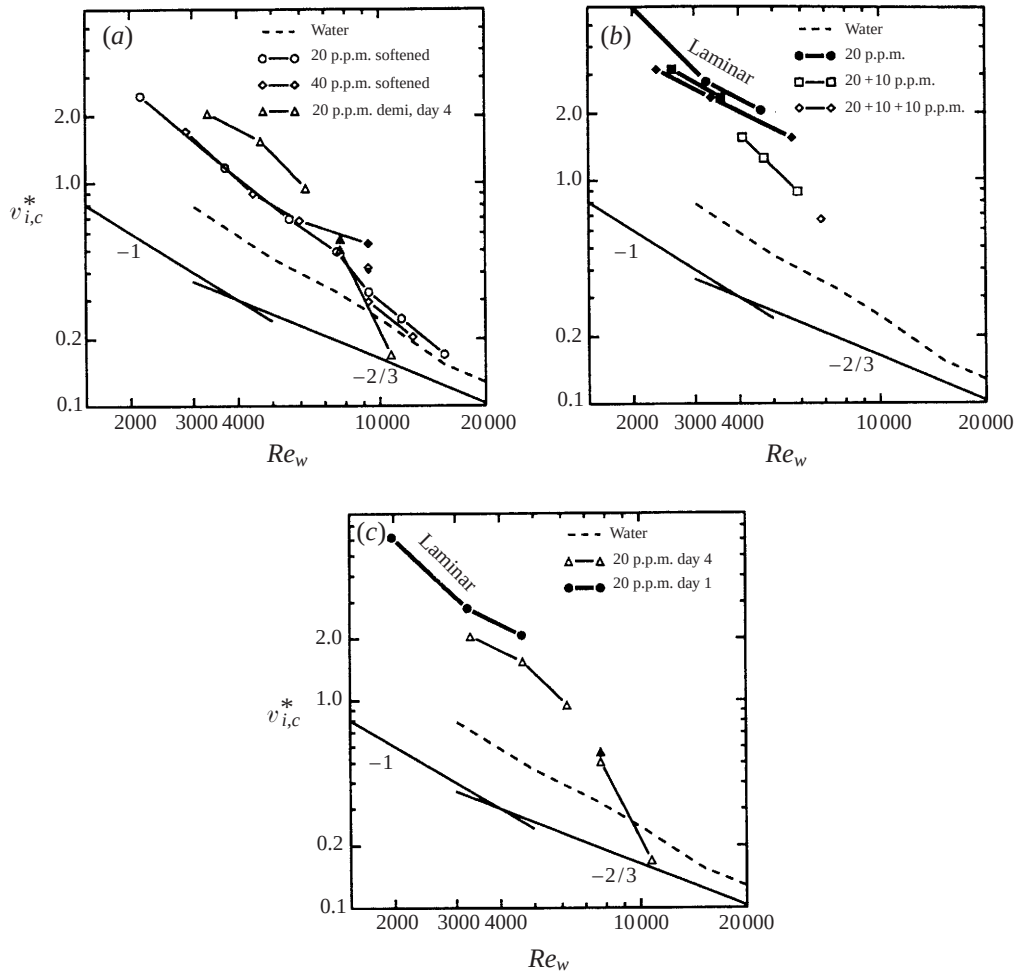

FIGURE 20. Critical relative disturbance velocity vs. Reynolds number for Superfloc A-110 solutions in various solvents for displacement volume $\Delta V = 174$ mm^3. Here, all solid symbols labelled 'laminar' indicate points where no transition could be triggered at the maximum disturbance velocity available, and are part of a line. Any unlabelled solid symbols indicate points where the flow relaminarizes if $v^*_{i,c}$ is increased in a multiple transition region.

number for 0.001 M. In this respect, it is also interesting to see that the 40 p.p.m. solution in softened water, which has a salt content in between that of the 0.001 M and the 0.01 M solution, indeed shows stabilizing behaviour in between results obtained for these two salt concentrations for low Reynolds numbers, as follows from in figure 19(*d*).

5. Main conclusions and discussion

In this final section we summarize the main results of our experimental study of the transition in circular pipe flow of both Newtonian and non-Newtonian fluids.

For the Newtonian fluid water, we have investigated triggered transition from laminar to turbulent flow up to Reynolds numbers of 50000. For $Re \leqslant 20000$, the flow has been found to be almost insensitive to the disturbance frequency or

alternatively to the dimensionless wavenumber α^*. Only for $\alpha^* \leqslant 5$, do we find a decrease in the dimensionless disturbance velocity $v_{i,c}^*$, an effect which is stronger for small Re. For $Re > 20\,000$, we find an increased sensitivity to disturbances with $\alpha^* \simeq 1$, an effect that becomes more pronounced at higher Reynolds numbers. There are indications that this behaviour is related to a second instability mode but no detailed measurements could be done to confirm this. For $Re \geqslant 30\,000$ and α^* varying from 2 to 6, we have found multiple transition points: this means that, when at constant α^* we increase the non-dimensional disturbance velocity v_i^*, we find a transition to turbulence at the lower critical value $v_{i,c}^*$, relaminarization at a larger $v_{i,c}^*$ and a second transition at the upper critical value, above which the flow remains turbulent. Perhaps this behaviour is related to an interaction between the artificially imposed disturbance and the very small natural disturbances that are present in the flow and which trigger natural transition at $Re > 60\,000$. Detailed measurements of the transitional flow structures using e.g. particle image velocimetry (PIV) techniques may reveal the origin of this surprising phenomenon.

In terms of scaling behaviour of transition, we find that for $\alpha^* \geqslant 5$ the critical disturbance velocity $v_{i,c}$ is practically independent of the Reynolds number, i.e. $v_{i,c}^*$ varies according to Re^{-1}. For $\alpha^* \leqslant 2$, however, the disturbance velocity $v_{i,c}^*$ depends on the Reynolds number according to $Re^{-2/3}$. This latter result is in agreement with theoretical studies (Davey & Nguyen 1971 and Sen *et al.* 1985). The neutrally stable three-dimensional nonlinear disturbance introduced by Smith & Bodonyi (1982) obeys a scaling of $Re^{-1/3}$ and is not in agreement with our findings. However, it should be mentioned that the shape of their helical wave disturbance is quite different from the one we have applied in our experiment. Development of a disturbance mechanism that generates a disturbance with the proper azimuthal wavenumber dependence (e.g. by placing more oscillating syringes in the circumferential direction), rather than the oscillating non-axisymmetric disturbance that we used in the present investigation, may help to check whether the disturbance proposed by Smith & Bodonyi exists.

The transition behaviour of non-Newtonian fluids is studied with help of polymer solutions. These are obtained by dissolving in water a minute amount of partially hydrolysed polyacrylamide (PAMH) which is a substance with a high molecular weight. It is found that the addition of polymers has a huge effect on the flow behaviour. In demineralized water, i.e. water without dissolved salts, PAMH has, on the average, an extended conformation. In this case, the viscosity of a 40 p.p.m. solution is increased more than ten times with respect to water at low shear rates. Also at these concentrations shear thinning is significant. Adding a small amount of salt causes the polymer to coil up. This results in a large decrease in viscosity and the shear thinning more or less disappears. Nevertheless, the change in viscosity, with respect to demineralized water, is still considerable and cannot be disregarded.

In addition to the change in viscosity, the polymers are also found to strongly reduce the natural transition Reynolds number from $Re > 60\,000$ for water to approximately 8000 for a fresh polymer solution with an extended conformation and to 30 000 for degraded as well as coiled polymer solutions. Similar effects have been reported by Paterson & Abernathy (1972). Natural transition originates from disturbances present in the entry section of the pipe. However, the exact cause of the reduction in natural transition Reynolds number by the polymers remains unsolved. One could speculate that the polymers change the flow in the contraction or have a destabilizing effect on the developing boundary layer in the entrance region of the pipe, perhaps similar to the destabilizing effect which elasticity has in a plane Poiseuille flow of an 'upper convected Maxwell' fluid (Porteous & Denn 1972*a*). Further research is needed and

for instance measurements of the velocity fields in the entry section of the pipe may clarify what causes this reduction in natural transition Reynolds number.

Although the polymers reduce the natural transition Reynolds number, our forced stability experiments show that larger disturbances are needed to trigger the transition to turbulence. This means that the polymers have a *stabilizing* effect on *developed* pipe flow. The stabilizing effect decreases with the concentration of salt in the water. In other words, the more the polymers are forced to have a coiled conformation the smaller their stabilizing influence becomes.

For randomly coiled polymers no *delay* in transition is found. In order to delay transition, our experiments show that the polymers need to have, on average, an extended conformation. This is consistent with findings by Virk & Wagger (1990) but they do not seem to have noticed the delay in transition as they concentrated only on the effect of drag reduction in their measurements. Our experiments suggest that the delay is mainly caused by the longest polymer molecules which is in agreement with White & McEligot (1970), who show that the delay in transition is dominated by the higher molecular weight polymers, while the effect on drag reduction is roughly additive.

Given the experimental data collected in this study, one may wonder whether it is possible to explain some results that have been reported previously in the literature. For instance, delay in transition for polymer solutions has been mainly reported in small diameter pipes, usually smaller than 1 cm (e.g. Castro & Squire 1967; White & McEligot 1970; Chung & Graebel 1972; Rochefort & Middleman 1985; Bewersdorff & Singh 1988). These results were found both for extended as well as coiled polymers. The latter result seems surprising in the light of our own experiments. An explanation can perhaps be given using scaling concepts. Let us introduce the Weissenberg number (We) as the ratio of the relaxation time of the polymer to the time scale of the flow, i.e.

$$We = \frac{U\lambda}{D} = Re\,E = Re\frac{\eta_0\lambda}{\rho D^2}. \tag{5.1}$$

It is clear that when for a given fluid and Reynolds number the pipe diameter is decreased, the Weissenberg number will rapidly increase. Moreover, from strongly nonlinear stability calculations for an 'upper convected Maxwell' fluid in two-dimensional plane Poiseuille flow we found that the influence of polymers is stabilizing beyond $We \approx 1$ (Draad 1996). Let us use this criterion also for a delay in transition: we then find that a delay in transition can be expected only when $We = 1$ occurs before the lowest transition Reynolds number $Re \approx 2300$. Thus, in small diameter pipes the polymers are likely to be stretched sufficiently by the laminar shear flow in order to lead to a delay in transition. Recently, a numerical simulation using a FENE-bead spring polymer model has shown that stretching of a coiled polymer in shear flows can indeed occur when the time scale related to the shear rate at the wall is smaller than the relaxation time of the polymer (Massah *et al.* 1993).

Extending these arguments to the large body of available literature on drag reduction also gives an explanation of why in most of these experiments, no change in transition Reynolds number has been reported. Namely, the vast majority of drag reduction experiments has been carried out in pipes with relatively large diameters in which the shear rate at the wall is insufficient to uncoil the polymers. The transition to turbulence then occurs at the same value as for Newtonian fluids. Once the turbulence becomes 'strong' enough so that it can stretch the polymers, drag reduction begins. This occurs at a so-called onset Reynolds number. The importance of stretched poly-

mers for drag reduction has been also demonstrated by den Toonder *et al.* (1997). The importance of extended polymers for a delay in the transition Reynolds number is also supported by linear stability theory (Landahl 1973 and Bark & Tinoco 1978) and experiments with long fibres (Vaseleski & Metzner 1974).

However, the results discussed above do not seem to be sufficient to clarify the total picture. We have found a delay in transition in our (large diameter) pipe only when the polymers are extended and fresh, i.e. undegraded (namely having a very large molecular weight). In such cases, the characteristic jump in friction factor normally present during transition is practically absent. Despite the smooth contraction and our careful pipe construction, the flow cannot be kept laminar far above this transition point. In this case, the minimum transition Reynolds number is thus almost equal to the maximum transition Reynolds number which is in sharp contrast with the results for Newtonian pipe flow and to a lesser extent for coiled and degraded polymer solutions. Somehow, the extended polymers seem to delay transition but at the same time generate their own instabilities to promote transition. The transition Reynolds number for such behaviour is denoted as $Re_{min/max}$. If such behaviour were to scale with the Weissenberg number according to (5.1), we could then shift $Re_{min/max}$ to lower values by using very small pipe diameters or by increasing the viscosity. This is precisely what has been found by e.g. Forame *et al.* (1972) and Zakin, Ni & Hansen (1977) and is known as 'early turbulence'. Forame *et al.* (1977) show that the onset wall shear stress for early turbulence varies slightly with the polymer concentration and depends almost linearly on the viscosity, i.e. the shear rate at the wall is constant whereas the critical Reynolds number varies between 600 and nearly 2000. This suggests that a delay in transition for extended high-molecular-weight polymers can only be found in large pipe diameters. Further research is required to confirm the suggested scaling.

We end by considering whether our data can be applied also to another type of substance, i.e. fibres. To try to formulate scaling rules for fibre suspensions based on a ratio of time scales is rather difficult. The equation describing the stresses in fibre suspensions is fully viscous and contains no characteristic time constant such as for the upper convected Maxwell fluid. The parameter B describing the stability behaviour of fibres (Bark & Tinoco 1978) contains only the aspect ratio of the fibre and the volume fraction occupied by the fibres. Thus, although fibre suspensions and extended polymers show similar behaviour with respect to drag reduction and transition to turbulence, the difference in the equation for the stresses points to a fundamental difference which is likely to be important when searching for scaling rules describing transition to turbulence for these materials.

Dr.ir. A. A. Draad has received financial support from Shell Research.

REFERENCES

Bark, F. H. & Tinoco, H. 1978 Stability of plane Poiseuille flow of a dilute suspension of slender fibres. *J. Fluid Mech.* **87**, 321–333.

Bergström, L. B. 1993 Optimal growth of small disturbances in pipe Poiseuille flow. *Phys. Fluids* A **5**, 2710–2720.

Bewersdorff, H. W. 1990 Drag reduction in surfactant solutions. In *Structure of Turbulence and Drag Reduction, IUTAM Symp. Zurich/Switzerland 1989* (ed. A. Gyr), pp. 293–312. Springer.

Bewersdorff, H. W. 1991 Turbulence structure of dilute polymer and surfactant solutions in artificially roughened pipes. In *6th European Drag Reduction Working Meeting, Eindhoven University of Technology, 21–22 November*.

Bewersdorff, H. W. & Singh, R. P. 1988 Turbulent drag reduction and relaminarization by Xanthan gum. In *Turbulence Management and Relaminarization, IUTAM Symposium Bangalore/India 1987*, pp. 333–348. Springer.

Bird, R. B., Armstrong, R. C. & Hassager, O. 1987*a* *Dynamics of Polymeric Liquids; Fluid Mechanics*, Second Edn, Vol. 1. John Wiley & Sons.

Bird, R. B., Curtiss, C. F., Armstrong, R. C. & Hassager, O. 1987*b* *Dynamics of Polymeric Liquids; Kinetic Theory*, Second Edn, Vol. 2. John Wiley & Sons.

Boere, J. W. R. A. 1995. Frequency and amplitude dependence of laminar-turbulent transition in pipe flow. Master Thesis MEAH-129. Delft University of Technology, Laboratory of Aero- & Hydrodynamics (in Dutch).

Castro, W. & Squire, W. 1967 The effect of polymer additives on transition in pipe flow. *Appl. Sci. Res.* **18**, 81–96.

Christiansen, E. B. & Lemmon, H. E. 1965 Entrance region flow. *AIChE J.* **11**, 995–999.

Chung, J. S. & Graebel, W. P. 1972 Laser anemometer measurements of turbulence in non-Newtonian pipe flows. *Phys. Fluids* **15**, 546–554.

Cohen, M. J. & Ritchie, N. J. B. 1962 Low-speed three-dimensional contraction design. *J. R. Aeronaut. Soc.* **66**, 231–236.

Darbyshire, A. G. & Mullin, T. 1995 Transition to turbulence in constant-mass-flux pipe flow. *J. Fluid Mech.* **289**, 83–114.

Davey, A. & Nguyen, H. P. F. 1971 Finite-amplitude stability of pipe flow. *J. Fluid Mech.* **45**, 701–720.

Draad, A. A. 1996 Laminar-turbulent transition in pipe flow for Newtonian and non-Newtonian fluids. PhD thesis, Delft University of Technology, Mechanical Engineering, The Netherlands.

Draad, A. A. & Nieuwstadt, F. T. M. 1998 The Earth's rotation and laminar pipe flow. *J. Fluid Mech.* **361**, 297–308.

Draad, A. A., Kuiken, G. D. C. & Nieuwstadt, F. T. M. 1995 Transition to turbulence in pipe flow. In *Laminar-Turbulent Transition, IUTAM Symp. Sendai/Japan 1994* (ed. R. Kobayashi), pp. 103–110. Springer.

Drazin, P. G. & Reid, W. H. 1981 *Hydrodynamic Stability*. Cambridge University Press.

Eliahou, S., Tumin, A. & Wygnanski, I. 1998 Laminar-turbulent transition in Poiseuille pipe flow subjected to periodic perturbation emanating from a wall. *J. Fluid Mech.* **361**, 333–349.

Forame, P. C., Hansen, R. J. & Little, R. C. 1972 Observations of early turbulence in the pipe pipe flow of drag reducing polymer solutions. *AIChE J.* **18**, 213–217.

Gordon, G. V. & Shaw, M. T. 1994 *Computer Programs for Rheologists.* Munich: Carl Hanser Verlag.

Groth, J. & Johansson, A. V. 1988 Turbulence reduction by screens. *J. Fluid Mech.* **197**, 139–155.

Hansen, R. J. 1973 Stability of laminar pipe flows of drag reduced polymer solutions in the presence of high-phase-velocity disturbances. *AIChE J.* **19**, 298–304.

Herbert, Th. 1983 Secondary instability of plane channel flow to subharmonic three-dimensional disturbances. *Phys. Fluids* **26**, 871–874.

Hua, S., Zhang, Z. & Nieuwstadt, F. T. M. 1998 Direct numerical simulation of a puff and slug in transitional cylindrical pipe flow. *J. Fluid Mech.* (submitted).

Kalashnikov, V. N. 1994 Shear-rate dependent viscosity of dilute polymer solutions. *J. Rheol.* **38**, 1385–1403.

Kleiser, L. & Zang, Th. A. 1991 Numerical simulation of transition in wall-bounded shear flows. *Ann. Rev. Fluid Mech.* **23**, 495–537.

Kozlov, V. V. & Ramazanov, M. P. 1984*a* Development of finite-amplitude disturbances in Poiseuille flow. *J. Fluid Mech.* **147**, 149–157.

Kozlov, V. V. & Ramazanov, M. P. 1984*b* Development of finite-amplitude disturbances in Poiseuille flow. In *IUTAM Symp. Laminar-Turbulent Transition* (ed. V. V. Kozlov).

Landahl, M. T. 1973 Drag reduction by polymer addition. In *Theoretical and Applied Mechanics, Proc. 13th Intl Congr. Theor. and Appl. Mech., Moscow 1972* (ed. E. Becker & G. K. Mikhailov), pp. 177–199. Springer.

Li, T.-Q. & McCarthy, K. L. 1995 Pipe flow of aqueous polyacrylamide solutions studied by means of nuclear magnetic resonance imaging. *J. Non-Newtonian Fluid Mech.* **57**, 155–175.

Massah, H., Kontomaris, W. R., Schowalter, W. R. & Hanratty, T. J. 1993 The configurations

of a FENE bead-spring chain in transient rheological flows and in a turbulent flow. *Phys. Fluids* A **5**, 881–890.

Maulik, B. K. 1989. Numerical studies of the Oldroyd-B fluid: Stability and transition in planar channels. PhD thesis, Princeton University, Department of Mechanical and Aerospace Engineering, USA.

Metzner, A. B. & Reed, J. C. 1955 Flow of non-Newtonian fluids – Correlation of the laminar, transition, and turbulent-flow regions. *AIChE J.* **1**, 434–440.

Nishioka, M., Iida, S. & Ichikawa, Y. 1975 An experimental investigation of the stability of plane Poiseuille flow. *J. Fluid Mech.* **72**, 731–751.

O'Sullivan, P. L. & Breuer, K. S. 1994*a* Transient growth in circular pipe flow. I. Linear disturbances. *Phys. Fluids* **6**, 3643–3651.

O'Sullivan, P. L. & Breuer, K. S. 1994*b* Transient growth in circular pipe flow. II. Nonlinear development. *Phys. Fluids* **6**, 3652–3664.

Paterson, R. W. & Abernathy, F. H. 1972 Transition to turbulence in pipe flow for water and dilute solution of polyethylene oxide. *J. Fluid Mech.* **51**, 177–185.

Porteous, K. C. & Denn, M. M. 1972*a* Linear stability of plane Poiseuille flow of viscoelastic liquids. *Trans. Soc. Rheol.* **16**, 295–308.

Porteous, K. C. & Denn, M. M. 1972*b* Nonlinear stability of plane Poiseuille flow of viscoelastic liquids. *Trans. Soc. Rheol.* **16**, 309–319.

Reynolds, O. 1883 An experimental investigation of the circumstances which determine whether the motion of water shall be direct or sinuous, and of the law of resistance in parallel channels. *Phil. Trans. R. Soc. Lond.* **174**, 935–982.

Rochefort, S. & Middleman, S. 1985 Effect of molecular configuration on Xanthan gum drag reduction. In *Polymer-Flow Interaction* (ed. Y. Rabin). American Institute of Physics, Conf. Proc. 137, pp. 333–348.

Rubin, Y., Wygnanski, I. & Haritonidis, J. H. 1980 Further observations on transition in a pipe. In *Laminar-Turbulent Transition, IUTAM Symp. Stuttgart/Germany 1979* (ed. R. Eppler & H. Fasel), pp. 17–26. Springer.

Sá Pereira, A. & Pinho, F. T. 1994 Turbulent pipe flow characteristics of low molecular weight polymer solutions. *J. Non-Newtonian Fluid Mech.* **55**, 321–344.

Schlichting, H. 1979 *Boundary-Layer Theory*, Seventh edn. McGraw-Hill.

Schmid, P. J. & Henningson, D. S. 1994 Optimal energy density growth in Hagen–Poiseuille flow. *J. Fluid Mech.* **277**, 197–225.

Sen, P. K., Venkateswarlu, D. & Maji, S. 1985 On the stability of pipe-Poiseuille flow to finite-amplitude axisymmetric and non-axisymmetric disturbances. *J. Fluid Mech.* **158**, 289–316.

Smith, F. T. & Bodonyi, R. J. 1982 Amplitude-dependent neutral modes in Hagen-Poiseuille flow through a circular pipe. *Proc. R. Soc. Lond.* A **384**, 463–489.

Sureshkumar, R. & Beris, A. N. 1995*a* Effect of artificial stress diffusivity on the stability of numerical calculations and the flow dynamics of time-dependent viscoelastic flows. *J. Non-Newtonian Fluid Mech.* **60**, 53–80.

Sureshkumar, R. & Beris, A. N. 1995*b* Linear stability analysis of viscoelastic Poiseuille flow using an Arnoldi-based orthogonalization algorithm. *J. Non-Newtonian Fluid Mech.* **56**, 151–182.

Tam, K. C. & Tiu, C. 1990 Role of ionic species and valency on the steady shear behaviour of partially hydrolysed polyacrylamide solutions. *Colloid & Polymer Sci.* **268**, 911–920.

Toonder, J. M. J. den, Draad, A. A., Kuiken, G. D. C. & Nieuwstadt, F. T. M. 1995 Degradation effects of dilute polymer solutions on turbulent drag reduction in pipe flows. *Appl. Sci. Res.* **55**, 63–82.

Toonder, J. M. J. den, Hulsen, M. A., Kuiken, G. D. C. & Nieuwstadt, F. T. M. 1997. Drag reduction by polymer additives in a turbulent pipe flow: numerical and laboratory experiment. *J. Fluid Mech.* **337**, 193–232.

Trefethen, L. N., Trefethen, A. E., Reddy, S. C. & Driscoll, T. A. 1993 Hydrodynamic stability without eigenvalues. *Science* **261**, 578–584.

Tumin, A. 1996 Receptivity of pipe Poiseuille flow. *J. Fluid Mech.* **315**, 119–137.

Vaseleski, R. C. & Metzner, A. B. 1974 Drag reduction in the turbulent flow of fibre suspensions. *AIChE J.* **20**, 301–306.

Virk, P. S. 1975 Drag reduction by collapsed and extended polyelectrolytes. *Nature* **253**, 109–110.

Virk, P. S. & Wagger, D. L. 1990 Aspects of mechanisms in type B drag reduction. In *IUTAM*

Symp. on Structure of Turbulence and Drag Reduction, Zurich/Switzerland 1989, pp. 201–213. Springer.

Virk, P. S., Merrill, E. W., Mickley, H. S., Smith, K. A. & Mollo-Christensen, E. L. 1967 The Toms phenomenon: turbulent pipe flow of dilute polymer solutions. *J. Fluid Mech.* **30**, 305–328.

Vlassopoulos, D. & Schowalter, W. R. 1994 Steady viscometric properties and characterization of dilute drag-reducing polymer solutions. *J. Rheol.* **38**, 1427–1446.

Waleffe, F. 1997 On a self-sustaining process in shear flows *Phys. Fluids* **9**, 883–900.

Walters, K. 1962 The solution of flow problems in the case of materials with memory. Part I. *J. Méc.* **1**, 479–486.

White, W. D. & McEligot, D. M. 1970 Transition of Mixtures of Polymers in a Dilute Aqueous Solution. *Trans. ASME*: *J. Basic Engng* September, 411–418.

Wójs, K. 1993 Laminar and turbulent flow of dilute polymer solutions in smooth and rough pipes. *J. Non-Newtonian Fluid Mech.* **48**, 337–355.

Wygnanski, I., Sokolov, M. & Friedman, D. 1975 On transition in a pipe. Part 2. The equilibrium puff. *J. Fluid Mech.* **69**, 283–304.

Wygnanski, I. J. & Champagne, F. H. 1973 On transition in a pipe. Part 1. The origin of puffs and slugs and the flow in a turbulent slug. *J. Fluid Mech.* **59**, 281–335.

Zakin, J. L., Ni, C. C. & Hansen, R. J. 1977 Laser Doppler velocimetry studies of early turbulence. *Phys. Fluids* **20**, s85–s88.